THE JOURNAL OF BIOLOGICAL CHEMISTRY VOL. 289, NO. 30, pp. 20939–20952, July 25, 2014

Cytoskeletal Reorganization Evoked by Rho-associated kinase- and Protein Kinase C-catalyzed Phosphorylation of Cofilin and Heat Shock Protein 27, Respectively, Contributes to Myogenic Constriction of Rat Cerebral Arteries*

Received for publication, January 27, 2014, and in revised form, June 3, 2014 Published, JBC Papers in Press, June 9, 2014, DOI 10.1074/jbc.M114.553743

Alejandro Moreno-Domínguez[‡1], Ahmed F. El-Yazbi[‡1,2], Hai-Lei Zhu[‡], Olaia Colinas[‡], X. Zoë Zhong[‡], Emma J. Walsh[‡], Dylan M. Cole[‡], Gary J. Kargacin[‡], Michael P. Walsh[§3], and William C. Cole[‡4]

From the Smooth Muscle Research Group, [‡]Departments of Physiology & Pharmacology and [§]Biochemistry & Molecular Biology, Libin Cardiovascular Institute and Hotchkiss Brain Institute, University of Calgary, Calgary, Alberta T2N 4N1, Canada

Background: The myogenic response of cerebral arteries to intravascular pressure regulates blood flow to the brain.
Results: Pressurization reduced smooth muscle G-actin and increased phospho-cofilin and -HSP27 content by a mechanism blocked by ROK or PKC inhibitors.
Conclusion: ROK- and PKC-mediated control of cofilin and HSP27 contributes to actin polymerization in myogenic constriction.
Significance: Knowledge of cytoskeletal dynamics is crucial for understanding myogenic control of cerebral arterial diameter.

Our understanding of the molecular events contributing to myogenic control of diameter in cerebral resistance arteries in response to changes in intravascular pressure, a fundamental mechanism regulating blood flow to the brain, is incomplete. Myosin light chain kinase and phosphatase activities are known to be increased and decreased, respectively, to augment phosphorylation of the 20-kDa regulatory light chain subunits (LC_{20}) of myosin II, which permits cross-bridge cycling and force development. Here, we assessed the contribution of dynamic reorganization of the actin cytoskeleton and thin filament regulation to the myogenic response and serotonin-evoked constriction of pressurized rat middle cerebral arteries. Arterial diameter and the levels of phosphorylated LC_{20}, calponin, caldesmon, cofilin, and HSP27, as well as G-actin content, were determined. A decline in G-actin content was observed following pressurization from 10 mm Hg to between 40 and 120 mm Hg and in three conditions in which myogenic or agonist-evoked constriction occurred in the absence of a detectable change in LC_{20} phosphorylation. No changes in thin filament protein phosphorylation were evident. Pressurization reduced G-actin content and elevated the levels of cofilin and HSP27 phosphorylation. Inhibitors of Rho-associated kinase and PKC prevented the decline in G-actin; reduced cofilin and HSP27 phosphoprotein content, respectively; and blocked the myogenic response. Furthermore, phosphorylation modulators of HSP27 and cofilin induced significant changes in arterial diameter and G-actin content of myogenically active arteries. Taken together, our findings suggest that dynamic reorganization of the cytoskeleton involving increased actin polymerization in response to Rho-associated kinase and PKC signaling contributes significantly to force generation in myogenic constriction of cerebral resistance arteries.

Blood flow to the brain is regulated through the interplay of multiple mechanisms that affect contractile force generation by vascular smooth muscle cells (VSMCs)[5] within the walls of cerebral resistance arteries and arterioles (1–4). Flow can be matched to metabolic demand under dynamic physiological conditions because these vessels develop contractile tone in response to intravascular pressure, referred to as the *myogenic response* (2). Myogenic tone development allows resistance vessels to achieve a state of partial constriction from which they can dilate or further constrict to alter flow in response to factors in the blood or released from surrounding cells, such as endothelial cells, neurons, and astrocytes (1–3). Our understanding of the molecular basis of myogenic constriction and how it is regulated by these vasoactive factors is incomplete.

A core concept of smooth muscle contraction is that cross-bridge cycling and force generation are a consequence of thick

* This work was supported by Canadian Institutes of Health Research Grants MOP-97988 and MOP-13505; fellowship awards from the Kertland Family Fellowship Fund & Andrew Family Professorship (to A. M.-D.), Alberta Heritage Foundation for Medical Research/Canadian Institutes of Health Research (to A. F. E.), the Spanish Ministry of Education (to O. C.), and Alberta Innovates-Health Solutions (to H.-L. Z.); and a Studentship award from Alberta Innovates-Health Solutions (to X. Z. Z.).
[1] These authors contributed equally to this work.
[2] Lecturer of Pharmacology at the Faculty of Pharmacy at Alexandria University.
[3] Alberta Heritage Foundation for Medical Research Scientist and recipient of a Canada Research Chair (Tier 1) in Vascular Smooth Muscle Research.
[4] Andrew Family Professor in Cardiovascular Research. To whom correspondence should be addressed: Smooth Muscle Research Group, Dept. of Physiology and Pharmacology, Libin Cardiovascular Inst. and Hotchkiss Brain Inst., Faculty of Medicine, University of Calgary, 3330 Hospital Dr. NW, Calgary, AB T2N 4N1, Canada. Tel.: 403-220-8885; Fax: 403-270-2211; E-mail: wcole@ucalgary.ca.

[5] The abbreviations used are: VSMC, vascular smooth muscle cell; MLCK, myosin light chain kinase; MLCP, myosin light chain phosphatase; LC_{20}, 20-kDa myosin regulatory light chain subunit; MYPT1, myosin light chain phosphatase targeting subunit 1; RMCA, rat middle cerebral artery; ROK, Rho-associated kinase; 5-HT, serotonin; HSP, heat shock protein; KRIBB3, 5-(5-ethyl-2-hydroxy-4-methoxyphenyl)-4-(4-methoxyphenyl)isoxazole; CyA, cyclosporin A.

filament regulation involving phosphorylation of 20-kDa myosin regulatory light chains (LC_{20}), with the level of phospho-LC_{20} dependent on the balance of myosin light chain kinase (MLCK) and phosphatase (MLCP) activities (5–8). Activation of actomyosin MgATPase activity and cross-bridge cycling in VSMCs is initiated by phosphorylation of LC_{20} at Ser-19 by MLCK. MLCK activity is $(Ca^{2+})_4$-calmodulin-dependent, and stimulated by a rise in cytosolic free Ca^{2+} concentration ($[Ca^{2+}]_i$) caused by membrane potential (E_m) depolarization and Ca^{2+} influx, or release from internal sarcoplasmic reticulum Ca^{2+} stores (5, 9). In contrast, LC_{20} dephosphorylation by MLCP is inhibited by Rho-associated kinase (ROK)-mediated phosphorylation of the MLCP targeting subunit MYPT1 (10–12) and PKC-mediated phosphorylation of the 17-kDa PKC-potentiated protein phosphatase 1 inhibitor protein, CPI-17 (13).

Appropriate regulation of MLCK and MLCP activities is necessary for the myogenic response. Myogenic constriction is accompanied by: (i) E_m depolarization leading to Ca^{2+} influx through voltage-gated Ca^{2+} channels (14), increased Ca^{2+} wave activity (*i.e.* increased frequency and number of cells exhibiting waves (15), but see (16)), and increased LC_{20} phosphorylation (17–19) that is suppressed by the MLCK inhibitor, ML-7 (17); as well as (ii) increased inhibitory MYPT1-T855 phosphorylation that is suppressed by blockers of ROK activity, including Y27632 and H1152, with an associated loss of myogenic constriction (18, 19). Although inhibition of PKC suppresses myogenic constriction (20, 21), no change in CPI-17 phosphorylation was detected, excluding a role for PKC-mediated suppression of MLCP activity (18, 19).

Although necessary for myogenic constriction, accumulating evidence indicates that mechanisms of MLCK and MLCP regulation are not sufficient (22). Additional mechanisms modulating force development include thin filament regulation (23) and dynamic reorganization of the actin cytoskeleton (24, 25). Calponin and caldesmon are thin filament-associated proteins that regulate smooth muscle contractility by directly inhibiting cross-bridge cycling (23, 26, 27). Phosphorylation of calponin reduces its inhibitory effect on cross-bridge cycling (28) and may account for slow cross-bridge cycling and contraction of smooth muscle cells in the absence of extracellular Ca^{2+} (29) and when LC_{20} phosphorylation is precluded by site-directed mutagenesis (30). Phosphorylation of caldesmon has similarly been linked to force generation in the absence of extracellular Ca^{2+} (31) and increased LC_{20} phosphorylation (32). Whether phosphorylation of calponin and/or caldesmon contributes to the myogenic response is unknown.

Several lines of evidence indicate that the cytoskeleton of smooth muscle cells is not a static structure; rather it is dynamically remodeled during contraction and relaxation (22, 24, 25, 33). Evidence of increased actin polymerization in the myogenic response was obtained for rat cerebral and tail arterial preparations (19, 34–37). Also, the myogenic response was affected by compounds that disrupt (cytochalasin D), prevent (latrunculin A or B), or enhance (jasplakinolide) actin polymerization (19, 34–38).

Actin filaments of the contractile apparatus are believed to be anchored to the cytoplasmic tails of integrins by a complex of membrane adhesion proteins and to each other at cytosolic dense bodies within the interior of VSMCs (25). Integrins, membrane adhesion complexes, and dense bodies are connected to each other and reinforced by the cortical actin cytoskeleton, and together these elements are thought to distribute and transmit force generated by the contractile apparatus over the cell membrane and to the extracellular matrix. Dynamic reorganization of the actin cytoskeleton during smooth muscle contraction is thought to involve expansion of adhesion protein complexes, severing of existing filaments to provide nucleation sites, and *de novo* actin polymerization of globular to filamentous actin (G- and F-actin, respectively) within the cortical actin network beneath the cell membrane (25, 39). This is postulated to strengthen the cytoskeleton and enhance force transmission from the contractile apparatus to the cell membrane and extracellular matrix (24, 25). Actin dynamics evoked by exposure to vasoconstrictor agonists involves a spatially restricted pool of nonmuscle γ- and β-actin within the cell cortex and at focal adhesions and dense bodies, but not smooth muscle α-actin that interacts with tropomyosin and forms the contractile actin filaments within the core of VSMCs (40, 41). Roles for additional cytoskeletal and membrane adhesion proteins in smooth muscle contraction have also been identified, including proteins such as talin that serve a structural role, and others that facilitate actin dynamics, such as the actin nucleation initiating factor, N-WASp (neuronal Wiskott-Aldrich Syndrome protein), cofilin, HSP20, HSP27, and VASP (vasodilator-stimulated phosphoprotein) (42–47).

Here, we employed pressurized rat cerebral arteries to assess the role of thin filament regulation and the contribution and regulation of actin polymerization in the myogenic response. No role for calponin or caldesmon regulation was detected. Force generation caused by actin polymerization was detected independent of a change in LC_{20} phosphorylation and cross-bridge cycling in the myogenic response and in vasoconstrictor-evoked contraction of myogenic arteries, accounting for ~30% of myogenic tone at 120 mm Hg. Evidence supporting a role for two regulators of actin dynamics, cofilin and HSP27, that are known to be regulated by ROK and PKC, respectively, was obtained.

EXPERIMENTAL PROCEDURES

Ethical Approval—Sprague-Dawley rats (250–275 g; Charles River, Montreal, Canada) were maintained and killed by halothane inhalation and exsanguination according to a protocol approved by the Animal Care Committee of the Faculty of Medicine of the University of Calgary and conforming to the standards of the Canadian Council on Animal Care. A total of 210 rats were employed.

Cerebral Arterial Pressure Myography—Rat brains were removed and transferred to ice-cold Krebs' saline solution containing 120 mM NaCl, 25 mM $NaHCO_3$, 4.8 mM KCl, 1.2 mM NaH_2PO_4, 1.2 mM $MgSO_4$, 11 mM glucose, 2.5 mM $CaCl_2$ (pH 7.4 when aerated with 95% air, 5% CO_2). Rat middle cerebral arteries (RMCAs) were dissected free of the surrounding connective tissue and cut into segments of 2–3 mm in length prior to cannulation and mounting in a pressure myograph system (Living Systems, Burlington, VT), as previously described (18).

The endothelial layer was disrupted by passing a stream of fine air bubbles through the vessel lumen and confirmed by the loss of vasodilatation to 10 μM bradykinin. External arterial diameter was measured using edge detection software (IonOptix, Milton, MA). Arteries were equilibrated at 10 mm Hg in warm Krebs' solution (37 ± 0.5 °C) for 15 min at the beginning of each experiment prior to an elevation of intraluminal pressure to 60 mm Hg to permit development of myogenic tone within 5–20 min. Arteries were then subjected to two 5-min pressure steps from 20 to 80 mm Hg to evoke a stable level of constriction (vessels exhibiting leaks or a lack of myogenic constriction were discarded). Intraluminal pressure was then set at 10 mm Hg for 10 min prior to the start of each experiment (pressure protocols for individual experiments are given under "Results"). Vessel segments from the same animal were used for control and treatment groups whenever possible to minimize vessel to vessel variability in phosphoprotein and G-actin quantification.

Circumferential Wall Stress Calculation—The circumferential wall stress (CWS) was calculated at radius r within the arterial wall using the following equation, from Coulson *et al.* (48), developed for a hollow cylinder subjected to uniform pressure

$$\mathrm{CWS}(r) = \frac{r_i^2 p_i}{r_e^2 - r_i^2}\left(1 + \frac{r_e^2}{r^2}\right) \qquad \text{(Eq. 1)}$$

where r is the radius, r_i is the internal radius, r_e is the external radius, and p_i is the internal pressure, respectively.

Protein Extraction—Vessels were frozen by rapid transfer to an ice-cold mixture of 10% trichloroacetic acid and 10 mM DTT in acetone prior to washing in acetone containing 10 mM DTT, lyophilization overnight, and storage at −80 °C. Prior to protein extraction, the cannulated ends were removed from each lyophilized vessel segment to avoid inclusion of tissue not subjected to test pressures prior to protein extraction in 60 μl of sample buffer (4% SDS, 100 mM DTT, 10% glycerol, 0.01% bromphenol blue, 60 mM Tris-HCl, pH 6.8). Each sample contained material from two to four pooled RMCA segments depending on the protein(s) of interest. Samples were heated at 95 °C for 10 min and rotated overnight at 4 °C prior to gel electrophoresis.

Phosphoprotein Western Blotting—A high sensitivity, three-step Western blotting method (18, 49) was used to quantify phosphorylation of LC_{20}, calponin (pan-antibody; 1:10,000), caldesmon (anti-S789; 1:250), HSP27 (anti-S82; 1:500), and cofilin (anti-S3; 1:500). Phosphorylated and unphosphorylated LC_{20} and calponin were separated by phosphate affinity tag (Phos-tag™) SDS-PAGE, transferred to PVDF membranes, and quantified as a percentage of total LC_{20} or calponin, respectively (49). Caldesmon, HSP27, and cofilin phosphorylation were detected using phosphoprotein-specific antibodies and normalized to actin content of each sample based on Johnson *et al.* (18), but the blocking agent was BSA.

G-actin Determination—G-actin content was determined for individual RMCA segments as previously described (50). Vessels were rapidly transferred to F-actin stabilization buffer (Cytoskeleton, Denver, CO) containing 50 mM PIPES (pH 6.9), 50 mM KCl, 5 mM $MgCl_2$, 5 mM EGTA, 5% (v/v) glycerol, 0.1% Nonidet P40, 0.1% Triton X-100, 0.1% Tween 20, 0.1% 2-mercaptoethanol, 0.001% antifoam C and then homogenized in 100 μl of stabilization buffer at room temperature. The homogenate was then centrifuged at 155,000 × g for 1 h at 22 °C to separate G- and F-actin; 30 μl of the high speed supernatant containing G-actin was carefully removed and added to 30 μl of 2× sample buffer. Samples were then heated at 95 °C for 10 min and stored at −20 °C prior to SDS-PAGE and Western blotting using a standard two-step protocol. SDS-PAGE was carried out in 1.5-mm-thick mini-gels (10% acrylamide in the resolving gel with 4.5% acrylamide stacking gel) at 30 mA for 1.5 h in a Mini Protean Cell (Bio-Rad). Following electrophoresis, proteins were transferred to a 0.2-μm nitrocellulose membrane at 100 V for 90 min at 4 °C, in transfer buffer containing 25 mM Tris-HCl, 192 mM glycine, and 20% methanol. Blotted membranes were washed in PBS for 5 min, incubated in 0.5% glutaraldehyde in PBS for 15 min to fix proteins on the membrane, and washed (twice for 5 min) with Tris-buffered saline containing Tween 20 (TBST: 20 mM Tris-HCl, pH 7.5, 137 mM NaCl, 3 mM KCl, 0.05% Tween 20). Membranes were blocked with 5% nonfat dried milk in TBS and 0.1% Tween 20 (0.1% TBST) for 1 h. After blocking, each membrane was cut at the 35-kDa molecular mass marker; the high molecular mass proteins were incubated with rabbit polyclonal anti-actin (1:1000 dilution), and the low molecular mass proteins were incubated with goat polyclonal anti-SM22α (1:2000 dilution). Both antibodies were incubated overnight at 4 °C in 1% dry milk in 0.1% TBST. Membranes were washed (four times for 5 min) in 0.1% TBST and incubated for 1 h in 1% dry milk and 0.1% TBST containing anti-rabbit IgG-HRP-conjugated secondary antibody (1:10,000 dilution) or donkey anti-goat IgG-HRP-conjugated secondary antibody (1:5000 dilution), respectively. After incubation with secondary antibody, membranes were washed (five times for 5 min) with TBST and (once for 5 min) with TBS before chemiluminescence signal detection using Amersham Biosciences ECL advanced Western blotting detection kit. The emitted light was detected and quantified with a chemiluminescence imaging analyzer (LAS3000 Mini; Fujifilm Canada, Mississauga, Canada), and images were analyzed with MultiGauge v3.0 software (Fujifilm Canada). Levels of G-actin were normalized to SM22 content, because SM22 is exclusively retained in the supernatant during high speed centrifugation (50) and expressed as a fraction of the level at 10 mm Hg.

Chemicals—All chemicals were purchased from Sigma unless indicated otherwise. Latrunculin B and GF109203X were obtained from Enzo Life Sciences (Plymouth Meeting, PA). Tween 20, Coomassie Brilliant Blue R250, TEMED, PVDF, and nitrocellulose membranes were from Bio-Rad. Polyclonal rabbit anti-LC_{20} and KRIBB3 (5-(5-ethyl-2-hydroxy-4-methoxyphenyl)-4-(4-methoxyphenyl)isoxazole) were from Santa Cruz Biotechnology (Santa Cruz, CA). Polyclonal rabbit anti-phospho-caldesmon-S789 was from Upstate (Charlottesville, VA). Polyclonal rabbit anti-phospho-HSP27-S82 was from Cell Signaling (Beverly, MA). Polyclonal goat anti-SM22-α was from Novus Biologicals (Littleton, CO). Polyclonal rabbit anti-calponin was prepared as described previously (51). Cyclosporin A, H1152, polyclonal rabbit anti-phospho-cofilin-S3, biotin-conjugated goat anti-rabbit, HRP-conjugated goat anti-rabbit, and HRP-conjugated donkey anti-goat secondary anti-

bodies were from EMD Millipore (Bellerica, MA), and HRP-conjugated streptavidin was from Pierce. Phos-tag™ acrylamide was from NARD Institute Ltd. (Amajasaki City, Japan).

Statistical Analysis—All values are presented as means ± S.E., with *n* values indicative of the number of vessels, or in the case of phosphoprotein and G-actin analysis, the number of samples (with two vessels pooled or a single vessel per sample, respectively) studied for each treatment. Statistical difference was determined using paired or unpaired Student's *t* test, analysis of variance, or repeated measures analysis of variance followed by Bonferoni's post hoc test as required. A p value of < 0.05 was considered to be statistically significant.

RESULTS

Decreased G-actin Content Associated with Myogenic- or Agonist-evoked Constriction in the Absence of Alterations in LC_{20}, Calponin, or Caldesmon Phosphorylation—RMCA constriction under conditions in which a detectable change in the level of LC_{20} phosphorylation was not apparent was specifically examined to assess the contribution of thin filament regulatory phosphoproteins and cytoskeletal reorganization to force development. Phospho-LC_{20} content of RMCAs pressurized to 100 mm Hg was previously shown to be ~50% (18), consistent with the maximal level of 50–55% detected for rat skeletal muscle arterioles pressurized to between 80 and 140 mm Hg (19). Based on these data, the level of phospho-LC_{20} was quantified using RMCA segments flash frozen at 10, 80, and 120 mm Hg once vessel diameter had stabilized at the relevant intraluminal pressure (this required 30 s to 3 min in different vessels). Fig. 1*A* shows a representative recording of arterial diameter during sequential pressure steps from 10 to 80 and 120 mm Hg. Pressure elevation from 80 to 120 mm Hg was associated with a reduction in the diameter of 17 ± 2.8 μm ($n = 9$ vessels; $p < 0.05$). Fig. 1*B* shows a representative Western blot of phosphorylated and unphosphorylated LC_{20} at 10, 80, and 120 mm Hg obtained using Phos-tag™ gels, and mean phospho-LC_{20} content was expressed as a percentage of total LC_{20} at 10, 80, and 120 mm Hg (± S.E.; $n = 14$, 9, and 7 arterial segments, respectively). No difference in phospho-LC_{20} content was observed for segments at 80 and 120 mm Hg, with levels of ~50% detected at both pressures ($p > 0.05$). Fig. 1 (*C* and *D*) shows representative Western blots and mean (± S.E.) levels of calponin and caldesmon phosphorylation at 80 and 120 mm Hg, respectively. No difference in calponin or caldesmon phosphorylation was evident at 80 and 120 mm Hg ($n = 3$ per group; $p > 0.05$ for both). In contrast, a significant reduction in G-actin content was detected. Fig. 1*E* shows representative blots of G-actin and SM22 content at 10, 80, and 120 mm Hg, as well as the mean level (± S.E.) of G-actin expressed as a fraction of the content at 10 mm Hg for vessels at 10, 80, and 120 mm Hg. Increasing pressure from 10 to 40 mm Hg did not evoke a significant change in G-actin content (data not shown), but a step from 10 to 80 caused G-actin levels to decline by ~66%, and a step from 80 to 120 mm Hg caused a further decline in G-actin content of ~21% ($n = 8$ for 10, 80, and 120 mm Hg, respectively; $p < 0.05$). Thus, the increased force generation at 120 compared with 80 mm Hg was associated with a reduction in G-actin content but no change in LC_{20} or thin filament regulatory protein phosphorylation.

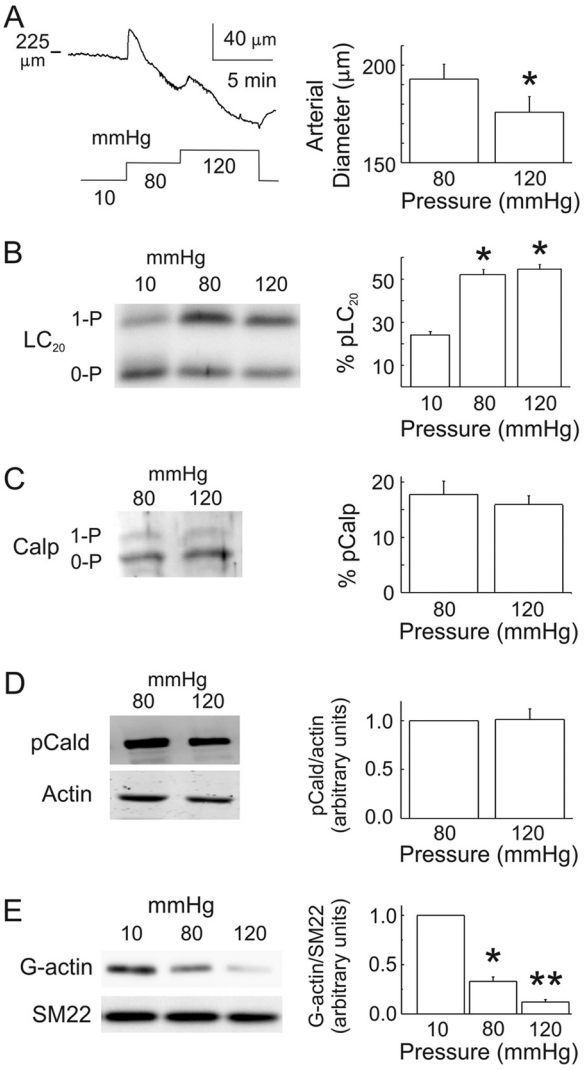

FIGURE 1. **Myogenic constriction evoked by pressure elevation from 80 to 120 mm Hg is associated with a decreased G-actin content but does not induce an increase in LC_{20}, calponin or caldesmon phosphorylation.** *A*, representative pressure-induced changes in RMCA diameter (*left panel*) and mean diameter (± S.E.; $n = 9$ vessels) (*right panel*) for RMCAs evoked by a step increase in pressure from 80 to 120 mm Hg in normal Krebs' solution. *B*, representative Western blot (*left panel*) and mean level ± S.E. of phospho-LC_{20} (pLC_{20}; *right panel*) as a percentage of total LC_{20} at 10, 80, and 120 mm Hg (respective *n* values of 14, 9, and 7; one or two arterial segments/sample) with monophosphorylated and unphosphorylated LC_{20} separated by Phos-tag™ SDS-PAGE. *C*, representative Western blot (*left panel*) and mean level ± S.E. of phospho-calponin (pCalp; *right panel*) as a percentage of total calponin at 80 and 120 mm Hg ($n = 3$; one or two arterial segments/sample) with monophosphorylated and unphosphorylated calponin separated by Phos-tag™ SDS-PAGE. *D*, representative Western blot of phospho-caldesmon (*pCald*) and corresponding levels of actin in each lane (*left*) and mean levels ± S.E. of normalized (to actin) phosphoprotein content at 120 mm Hg expressed as a fraction of the value at 80 mm Hg (*right*) ($n = 3$; one or two arterial segments/sample). *E*, representative Western blot of G-actin and corresponding SM22 content in each lane (*left panel*) and mean levels ± S.E. of G-actin normalized to SM22 at 80 and 120 mm Hg expressed as a fraction of the value at 10 mm Hg (*right panel*) ($n = 8$; one arterial segment per sample). *, significantly different ($p < 0.05$) from value at 80 (*A*) or 10 mm Hg (*B* and *E*). **, significantly different ($p < 0.05$) from value at 80 mm Hg (*E*).

An identical maximal level of LC_{20} phosphorylation of ~50% was previously detected in RMCAs exposed to 1, 3, or 10 μM 5-HT at 10 mm Hg (52). Based on these data, we quantified the

changes in LC_{20}, calponin, and caldesmon phosphoprotein and G-actin content caused by pressurization from 10 to 80 mm Hg in the presence of 5-HT (1 μM), or in the reverse situation, during exposure to 5-HT (1 μM) after stable development of myogenic tone at 80 mm Hg. Fig. 2*A* shows representative recordings of arterial diameter for RMCAs treated with 5-HT at 10 mm Hg in the absence or presence of a subsequent pressure step to 80 mm Hg. Notably, the pressure step from 10 to 80 mm Hg after 5-HT treatment evoked myogenic tone development as indicated by the presence of an initial dilation followed by constriction of 25 ± 5 μm ($n = 6$ vessels; $p < 0.05$). No difference in LC_{20}, calponin, or caldesmon phosphorylation was detected, but a significant 63 ± 11% decline in the level of G-actin was evident in vessels exposed to 5-HT and then pressurized to 80 from 10 mm Hg (Fig. 2, *B* ($n = 6$ vessels/group) and *C–E* ($n = 3$ vessels/group)). A similar decline in G-actin content in the absence of a change in phosphoprotein content was also associated with the vasoconstriction of RMCAs treated with 5-HT at 80 mm Hg. Fig. 3*A* shows representative recordings of RMCA diameter during a step increase in pressure from 10 to 80 mm Hg alone and an identical pressure step followed by 5-HT (1 μM). Although vasoconstriction of ~35 μm (215 ± 8 *versus* 180 ± 11 μm; $n = 7$ vessels, $p < 0.05$) was evident on exposure to 5-HT, no difference in LC_{20}, calponin, or caldesmon phosphorylation was detected in the presence compared with the absence of 5-HT at 80 mm Hg (Fig. 3, *B* ($n = 5$ vessels/group) and *C* and D ($n = 3$ vessels/group); $p > 0.05$ in each case). However, the vasoconstriction to 5-HT at 80 mm Hg was associated with a significant decline of 61.5 ± 5.5% in G-actin content ($n = 4$; $p < 0.05$). Notably, the values for the final diameter prior to freezing and magnitude of decline in G-actin content at 80 mm Hg in the presence of 5-HT were not different regardless of the order of pressurization and agonist exposure ($p > 0.05$).

The initial spontaneous development of myogenic tone by RMCAs during equilibration at 60 mm Hg typically requires 5–20 min (Fig. 4*A*, *left panel*). Fig. 4*B* shows that no detectable difference in the level of LC_{20} phosphorylation was apparent when RMCAs were flash frozen prior to tone development (Fig. 4*A*, *right panel*) compared with vessels frozen at ~20 min when stable myogenic constriction was achieved. In contrast, G-actin content was different before and after tone development at 60 mm Hg (Fig. 4*C*). Specifically, the level of G-actin detected before tone development was identical to that at 10 mm Hg, but it was ~60% lower after stable tone was achieved ($p < 0.05$; $n =$ 5 per group).

We next determined whether the pressure-evoked decline in G-actin content of RMCAs was sensitive to modulators of the actin cytoskeleton and/or cross-bridge cycling. Treatment with latrunculin B (10 μM) to sequester G-actin did not affect RMCA diameter at 10 mm Hg (data not shown), but it did cause a significant vasodilatation at 80 mm Hg (Fig. 5*A*). The loss of tone at 80 mm Hg in latrunculin B was not associated with a decline in LC_{20} phosphorylation, but a significant ~4-fold increase in G-actin content was detected (Fig. 5, *B* and *C*). Latrunculin B similarly evoked dilation of vessels treated with 5-HT at 80 mm Hg or pressurized to 80 mm Hg after 5-HT

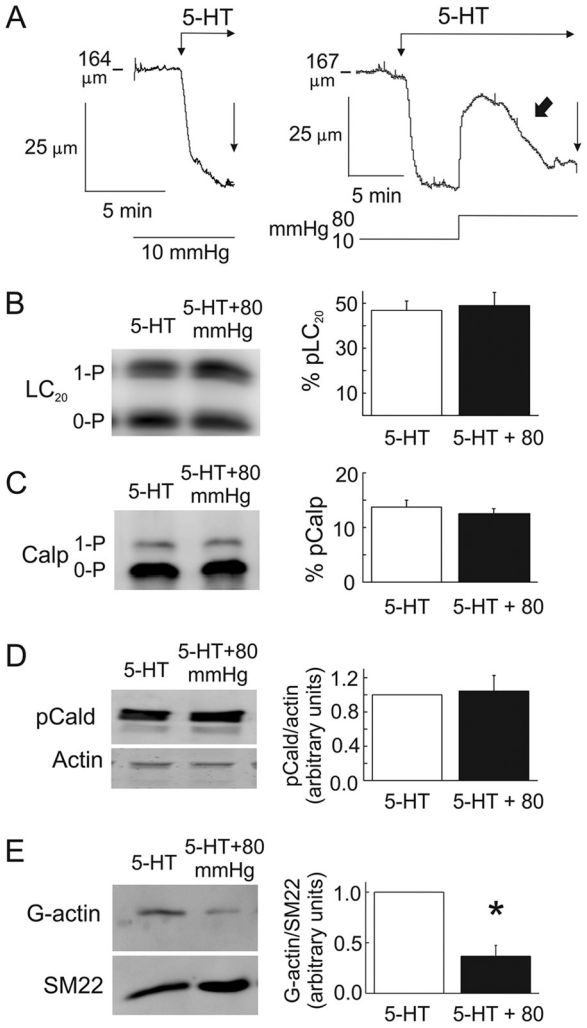

FIGURE 2. **Myogenic constriction at 80 mm Hg in the presence of 5-HT is accompanied by decreased G-actin content, but no change in LC_{20}, calponin, or caldesmon phosphorylation.** *A*, representative recordings of RMCA diameter during the application of 5-HT (1 μM) and during a step increase in pressure from 10 to 80 mm Hg following the application of 5-HT. The *thick arrow* indicates the presence of myogenic constriction in the presence of 5-HT, and thin vertical arrows at the end of each trace indicate the point of flash freezing for biochemical analysis. *B*, representative Western blot (*left panel*) and mean level ± S.E. of phospho-LC_{20} (pLC_{20}; *right panel*) as a percentage of total LC_{20} in 5-HT at 10 mm Hg and at 80 mm Hg in the continued presence of 5-HT ($n = 6$; one or two arterial segments/sample) with monophosphorylated and unphosphorylated LC_{20} separated by Phos-tag™ SDS-PAGE. *C*, representative Western blot (*left panel*) and mean level ± S.E. of phospho-calponin (pCalp; *right panel*) as a percentage of total calponin in 5-HT at 10 mm Hg and at 80 mm Hg in the continued presence of 5-HT ($n = 3$; one or two arterial segments/sample) with monophosphorylated and unphosphorylated calponin separated by Phos-tag™ SDS-PAGE. *D*, representative Western blot of phospho-caldesmon (*pCald*) and corresponding levels of actin in each lane (*left panel*) and mean levels ± S.E. of normalized (to actin) phosphoprotein content at 80 mm Hg in the presence of 5-HT expressed as a fraction of the value in 5-HT at 10 mm Hg (*right panel*) ($n = 3$; one or two arterial segments/sample). *E*, representative Western blot of G-actin and corresponding SM22 content in each lane (*left panel*) and mean levels ± S.E. of G-actin normalized to SM22 at 80 mm Hg in the presence of 5-HT expressed as a fraction of the value in 5-HT at 10 mm Hg (*right panel*) ($n = 3$; one arterial segment per sample). *, significantly different ($p < 0.05$) from value in 5-HT at 10 mm Hg.

treatment (Fig. 6, *B* and *C*), but not in vessels treated with 5-HT at 10 mm Hg (Fig. 6*A*).

Previous work indicated that microcystin (phosphatase inhibitor)-triggered LC_{20} phosphorylation in permeabilized rat

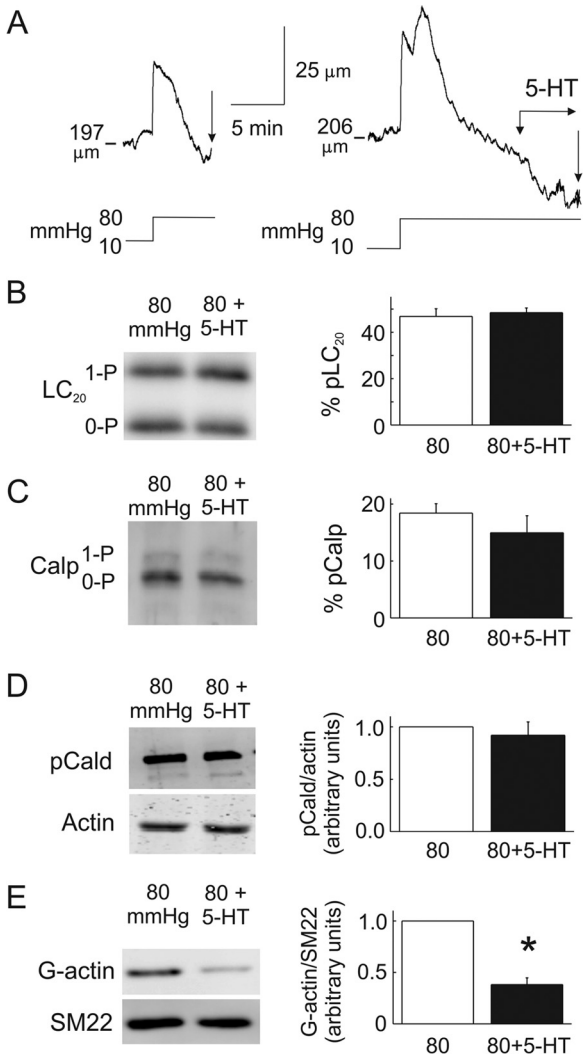

FIGURE 3. **5-HT-evoked constriction at 80 mm Hg is associated with a decreased G-actin content, but no change in LC_{20}, calponin, or caldesmon phosphorylation.** *A*, representative recordings of RMCA diameter during a step increase in pressure from 10 to 80 mm Hg and during a similar increase in pressure followed by 5-HT (1 μM). *Vertical arrows* at the end of each trace indicate the point of flash freezing for biochemical analysis. *B*, representative Western blot (*left panel*) and mean level ± S.E. of phospho-LC_{20} (pLC_{20}; *right panel*) as a percentage of total LC_{20} at 80 mm Hg ± 5-HT ($n = 5$; one or two arterial segments/sample) with monophosphorylated and unphosphorylated LC_{20} separated by Phos-tag™ SDS-PAGE. *C*, representative Western blot (*left panel*) and mean level ± S.E. of phospho-calponin (pCalp; *right panel*) as a percentage of total calponin at 80 mm Hg ± 5-HT ($n = 3$; one or two arterial segments/sample) with monophosphorylated and unphosphorylated calponin separated by Phos-tag™ SDS-PAGE. *D*, representative Western blot of phospho-caldesmon (*pCald*) and corresponding levels of actin in each lane (*left panel*) and mean levels ± S.E. of normalized (to actin) phosphoprotein content in 5-HT at 80 mm Hg expressed as a fraction of the value at 80 mm Hg (*right panel*) ($n = 3$; one or two arterial segments/sample). *E*, representative Western blot of G-actin and corresponding SM22 content in each lane (*left panel*) and mean levels ± S.E. of G-actin normalized to SM22 in 5-HT at 80 mm Hg expressed as a fraction of the value at 80 mm Hg (*right panel*) ($n = 4$; one arterial segment per sample). *, significantly different ($p < 0.05$) from value at 80 mm Hg.

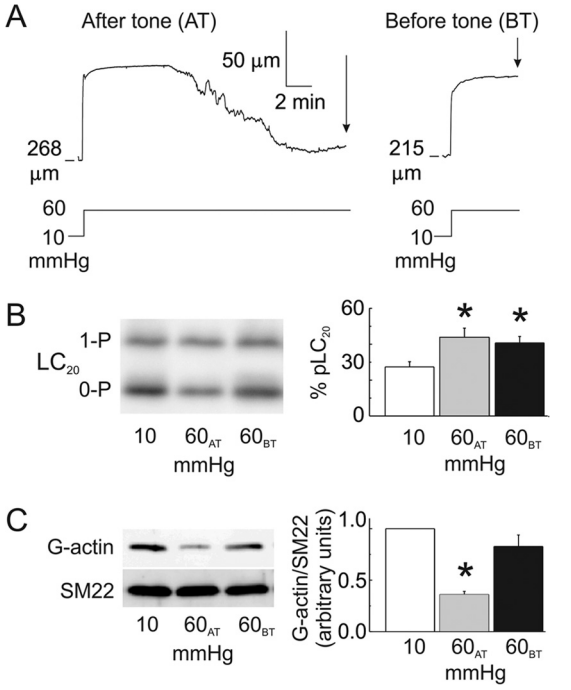

FIGURE 4. **Spontaneous development of myogenic tone during equilibration is associated with a decrease in G-actin content, but no change in LC_{20} phosphorylation.** *A*, representative recordings of RMCA diameter during equilibration at 60 mm Hg showing spontaneous tone development in Krebs' solution (after tone, *AT*) and an identical vessel that was flash frozen prior to tone development (before tone, *BT*). *Vertical arrows* indicate flash freezing for biochemical analysis. *B*, representative Western blot (*left panel*) and mean levels ± S.E. of phospho-LC_{20} (pLC_{20}; *right panel*) as a percentage of total LC_{20} at 10, 60 (*AT*), and 60 (*BT*) mm Hg ($n = 4$; one or two arterial segments/sample) with monophosphorylated and unphosphorylated LC_{20} separated by Phos-tag™ SDS-PAGE. *C*, representative Western blot of G-actin and corresponding SM22 content in each lane (*left panel*) and mean levels ± S.E. of G-actin normalized to SM22 at 60 (*AT*) and 60 (*BT*) mm Hg expressed as a fraction of the value at 10 mm Hg (*right panel*) ($n = 5$; one arterial segment per sample). *, significantly different ($p < 0.05$) from value at 10 mm Hg.

mesenteric arteries evoked increased actin polymerization, whereas depolymerization was observed if LC_{20} phosphorylation was suppressed with the MLCK inhibitor ML-7, suggesting interplay between the extent of LC_{20} phosphorylation and the level of actin polymerization (53). To test this possible mechanism in the myogenic response, we used blebbistatin, which potently inhibits the actin-activated ATPase activity of mammalian smooth muscle myosin II without affecting myosin phosphorylation (54). RMCAs were treated with blebbistatin (20 μM), before or after induction of the myogenic response, and vessel diameter and G-actin content were measured. The addition of blebbistatin after the pressure jump reversed the myogenic response but had no effect on the pressure-induced actin polymerization (Fig. 7*A*). When added at 10 mm Hg, prior to increasing intraluminal pressure to 120 mm Hg, blebbistatin had no effect on vessel diameter at 10 mm Hg, and the vessel dilated when the pressure was increased to 120 mm Hg in the presence of blebbistatin, *i.e.* the myogenic response at 120 mm Hg was abolished (Fig. 7*B*, *top panel*). Most importantly, as shown in the *middle* and *bottom panels* of Fig. 7*B*, blebbistatin did not affect the pressure-induced actin polymerization. These results suggest that force generation *per se* was not responsible for the decline in G-actin content; *i.e.* there was no evidence of interplay between the extent of LC_{20} phosphorylation and the level of actin polymerization.

Contribution of ROK- and PKC-mediated Cytoskeletal Reorganization Involving Cofilin and HSP27 Phosphorylation in the Myogenic Response of RMCAs—The lack of a direct effect of force generation on G-actin content suggested the possibility that cellular signaling was likely involved in initiating the

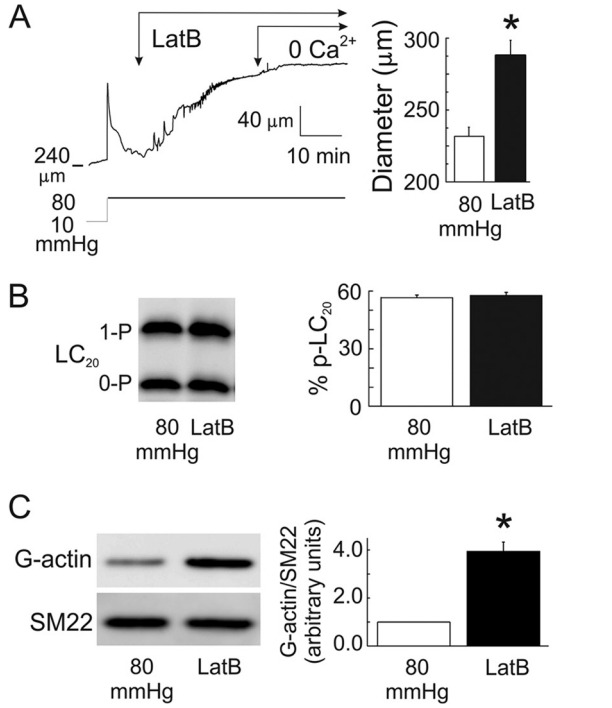

FIGURE 5. **Pressure-evoked reduction in G-actin content is blocked by latrunculin B.** *A*, representative recording of RMCA diameter (*left panel*) and mean diameter (± S.E.; $n = 6$; *right panel*) during a step increase in pressure from 10 to 80 mm Hg followed by sequential treatment with latrunculin B (*LatB*) (10 μM) and zero extracellular Ca^{2+} solution (0 Ca^{2+}) at 80 mm Hg. *B*, representative Western blot (*left panel*) and mean level ± S.E. of phospho-LC_{20} (pLC_{20}; *right panel*) as a percentage of total LC_{20} at 80 mm Hg ± latrunculin B ($n = 3$; one or two arterial segments/sample) with monophosphorylated and unphosphorylated LC_{20} separated by Phos-tag™ SDS-PAGE. *C*, representative Western blot of G-actin and corresponding SM22 content in each lane (*left panel*) and mean levels ± S.E. of G-actin normalized to SM22 at 80 mm Hg in latrunculin B expressed as a fraction of the value at 80 mm Hg (*right panel*) ($n = 4$; one vessel per sample). *, significantly different ($p < 0.05$) from value at 80 mm Hg (*A* and *C*).

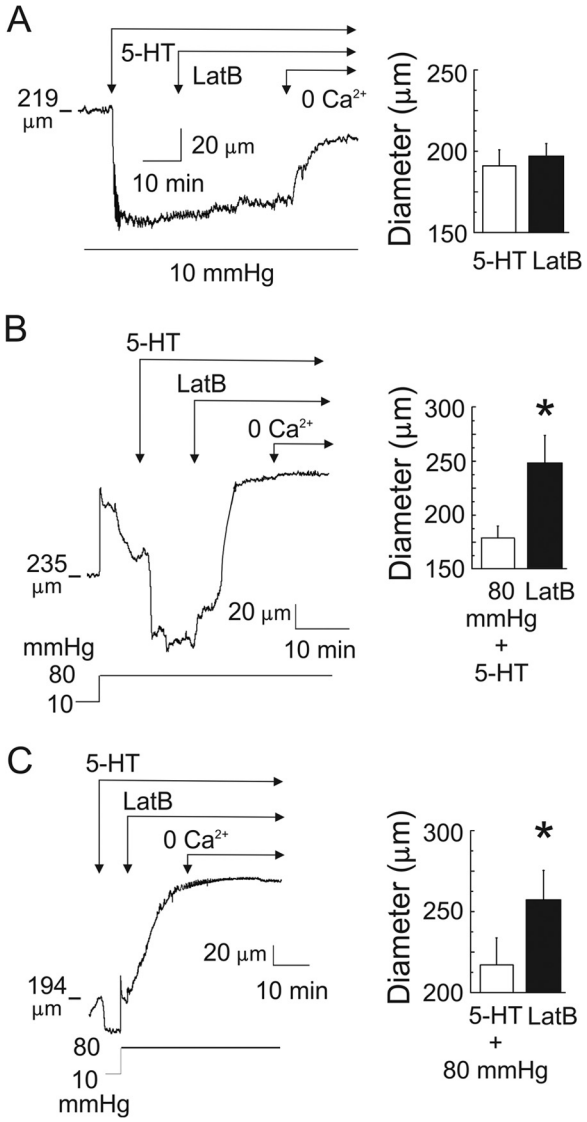

FIGURE 6. **Sequestration of G-actin with latrunculin B is accompanied by full dilation of RMCAs treated with 5-HT at 80 mm Hg or pressurized to 80 mm Hg after 5-HT treatment.** *A*, representative recording of RMCA diameter (*left panel*) during sequential exposure to 5-HT (1 μM), latrunculin B (*LatB*) (10 μM), and zero extracellular Ca^{2+} solution (0 Ca^{2+}) at 10 mm Hg and mean diameter (± S.E.; $n = 6$; *right panel*) in 5-HT at 10 mm Hg ± latrunculin B. *B*, representative recording of RMCA diameter (*left*) during a step increase in pressure from 10 to 80 mm Hg followed by sequential treatment with 5-HT (1 μM), latrunculin B (*LatB*) (10 μM), and zero extracellular Ca^{2+} solution (0 Ca^{2+}) at 80 mm Hg and mean diameter (± S.E.; $n = 7$; *right panel*) in 5-HT at 80 mm Hg ± latrunculin B. *C*, representative recording of RMCA diameter (*left panel*) during treatment with 5-HT followed by a step increase in pressure from 10 to 80 mm Hg, latrunculin B, and zero extracellular Ca^{2+} solution in the continued presence of 5-HT and mean diameter (± S.E.; $n = 7$; *right panel*) in 5-HT at 80 mm Hg ± latrunculin B. *, significantly different ($p < 0.05$) from the value in the absence of latrunculin B.

remodeling mechanism. For this reason, we assessed the contribution of ROK and PKC signaling pathways and two potential regulators of cytoskeletal reorganization, cofilin and HSP27, that are downstream of ROK and PKC, respectively. Fig. 8 indicates the effect of ROK and PKC inhibition by H1152 (0.5 μM) and GF109203X (3 μM) treatment, respectively, on the level of G-actin at 120 mm Hg. RMCAs were pressurized to 120 mm Hg, and H1152 or GF109203X was then applied when stable myogenic tone was observed. Both inhibitors caused a loss of myogenic tone and dilatation, as previously reported (18, 19, 52). G-actin content in the presence of H1152 or GF109203X was significantly elevated compared with that of untreated RMCAs at 120 mm Hg and not different from that detected at 10 mm Hg ($p > 0.05$; $n = 4$ per group), consistent with the view that ROK and PKC mediate cytoskeletal reorganization in the myogenic response.

Two cytoskeleton-associated proteins, cofilin and HSP27, were previously identified as potential mediators of ROK- and PKC-dependent control of actin polymerization in smooth muscle contraction (44, 55, 56), but their role in the myogenic response of resistance arteries has not been assessed. Fig. 9 shows the pressure-dependent changes in, and the effects of ROK and PKC inhibition on, the levels of cofilin-S3 and HSP27-S82 phosphorylation associated with myogenic constriction at 120 mm Hg ($n = 6$ per group). Pressurization to 120 from 10 mm Hg was associated with ~2.7- and ~2.5-fold increased levels of phospho-HSP27-S82 and phospho-cofilin-S3, respectively. GF109203X suppressed the pressure-dependent increase in HSP27-S82 phosphorylation at 120 mm Hg to a level similar to that in untreated vessels at 10 mm Hg (Fig. 9, *A* and *B*). However, GF109203X did not affect phospho-cofilin-S3 content (Fig. 9, *A* and *C*). In contrast, suppression of ROK activity with H1152 blocked the pressure-dependent increase in cofilin-S3, but not HSP27-S82 phosphorylation at 120

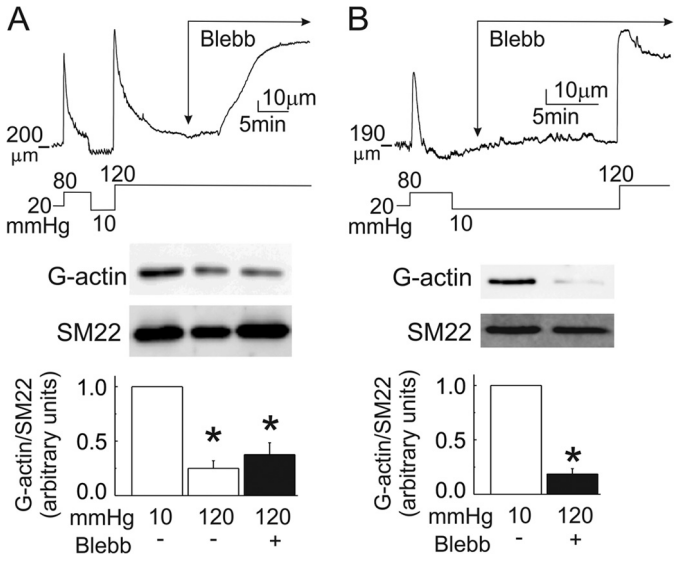

FIGURE 7. **Pressure-evoked reduction in G-actin content is not affected by blebbistatin treatment.** *A*, representative recording (*top panel*) of RMCA diameter during treatment with blebbistatin (*Blebb*) (20 μM) after a pressure step from 10 to 120 mm Hg. Representative Western blot of G-actin and corresponding SM22 content in each lane (*middle panel*) and mean levels ± S.E. of G-actin normalized to SM22 at 120 mm Hg ± blebbistatin expressed as a fraction of the value at 10 mm Hg (*bottom panel*) ($n = 3$; one vessel per sample). *B*, representative recording (*top panel*) of RMCA diameter during treatment with blebbistatin before a pressure step from 10 to 120 mm Hg. Representative Western blot of G-actin and corresponding SM22 content in each lane (*middle panel*) and mean levels ± S.E. of G-actin normalized to SM22 at 120 mm Hg in the presence of blebbistatin expressed as a fraction of the value at 10 mm Hg (*bottom panel*) ($n = 3$; one vessel per sample). *, significantly different ($p < 0.05$) from value at 10 mm Hg.

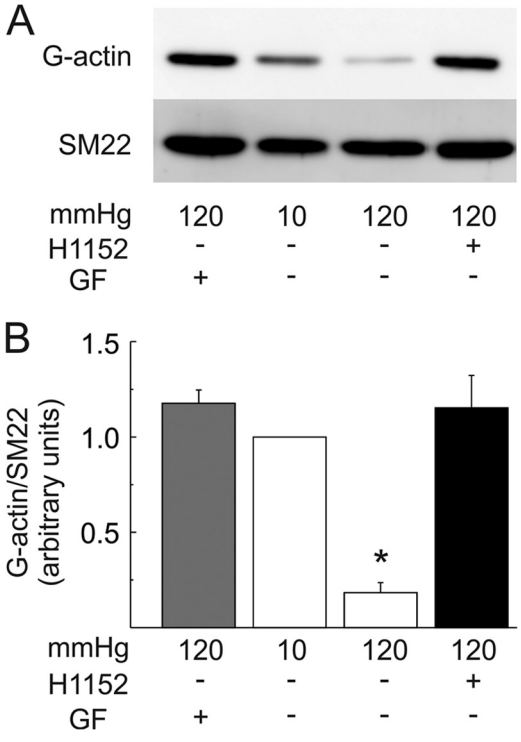

FIGURE 8. **Decline in G-actin content in the myogenic response is blocked by inhibitors of PKC- and ROK-dependent signaling.** *A*, representative Western blot of G-actin and corresponding SM22 content in each lane. *B*, mean levels ± S.E. of G-actin normalized to SM22 of RMCAs at 120 mm Hg ± H1152 (0.5 μM) or GF109203X (GF; 3 μM) expressed as a fraction of the value at 10 mm Hg ($n = 4$ blots with one arterial segment per sample). *, significantly different ($p < 0.05$) from value at 10 mm Hg.

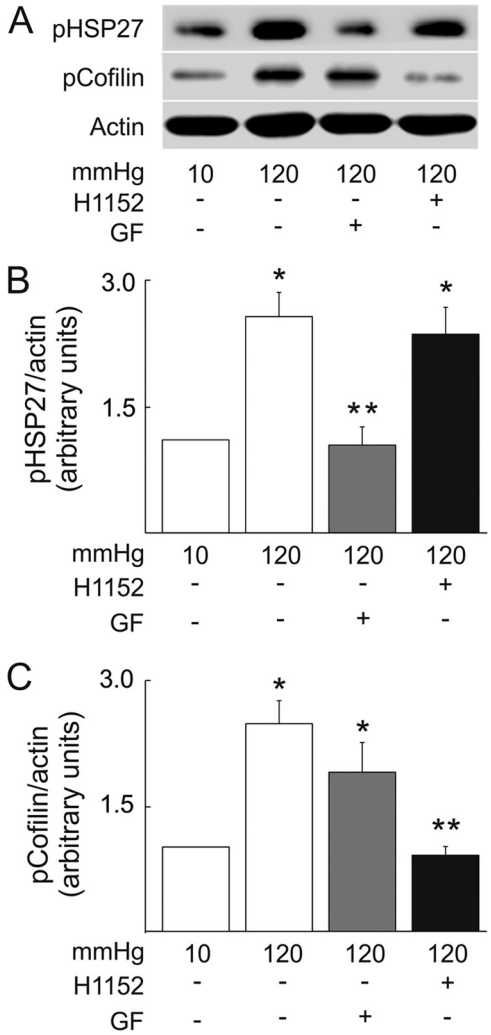

FIGURE 9. **Pressure elevation evokes increased HSP27-S82 and cofilin-S3 phosphorylation via PKC- and ROK-dependent signaling, respectively.** *A*, representative Western blots of phospho-HSP27 and phospho-cofilin and corresponding levels of actin in each lane. *B* and *C*, mean levels ± S.E. of normalized (to actin) phosphoprotein content of RMCAs at 120 mm Hg ± H1152 (0.5 μM) or GF109203X (*GF*; 3 μM), respectively, expressed as a fraction of the value at 10 mm Hg (*B* and *C*) ($n = 6$ blots with three arterial segments/sample). *, significantly different ($p < 0.05$) from value at 10 mm Hg. **, significantly different ($p < 0.05$) from value at 120 mm Hg.

mm Hg. The level of phospho-cofilin-S3 in H1152 was similar to that in untreated vessels at 10 mm Hg (Fig. 9, *A* and *C*). The present finding of increased cofilin phosphorylation in the myogenic response differs from previous reports showing decreased levels of phospho-cofilin in tracheal and conduit arterial smooth muscle treated with constrictor agonists (44, 56). For this reason, we performed an additional set of experiments in which RMCAs were exposed to 5-HT (1 μM) at 10 mm Hg. The level of phospho-cofilin was increased by 2.4 ± 0.4-fold in 5-HT compared with untreated vessels ($n = 6$ in each group; $p < 0.05$; Fig. 10). We also tested the effects of KRIBB3 (10 μM), which inhibits PKC-dependent HSP27 phosphorylation, and cyclosporin A (CyA) (10 μM), a phosphatase 2B (type 2B protein serine/threonine phosphatase (calcineurin)) inhibitor. Fig. 11 shows that KRIBB3 suppressed the pressure-dependent increase in HSP27-S82 phosphorylation at 60 mm Hg (Fig. 11, *A* and *B*), with no effect on the phospho-cofilin-S3 content (Fig. 11, *A* and *C*). CyA, on the other hand, enhanced significantly

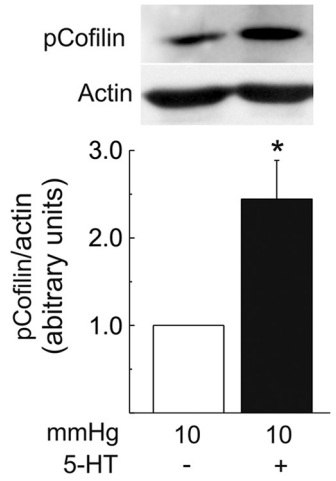

FIGURE 10. **5-HT-evoked increase in cofilin-S3 phosphorylation in RMCAs at 10 mm Hg.** Show are representative Western blots of phospho-cofilin and corresponding levels of actin in each lane (*upper panel*) and mean levels ± S.E. of normalized (to actin) phosphoprotein content of RMCAs at 10 mm Hg ± 5-HT (1 μM) expressed as a fraction of the value at 10 mm Hg (*lower panel*) (n = 6 blots with three arterial segments/sample). *, significantly different ($p < 0.05$) from value at 10 mm Hg.

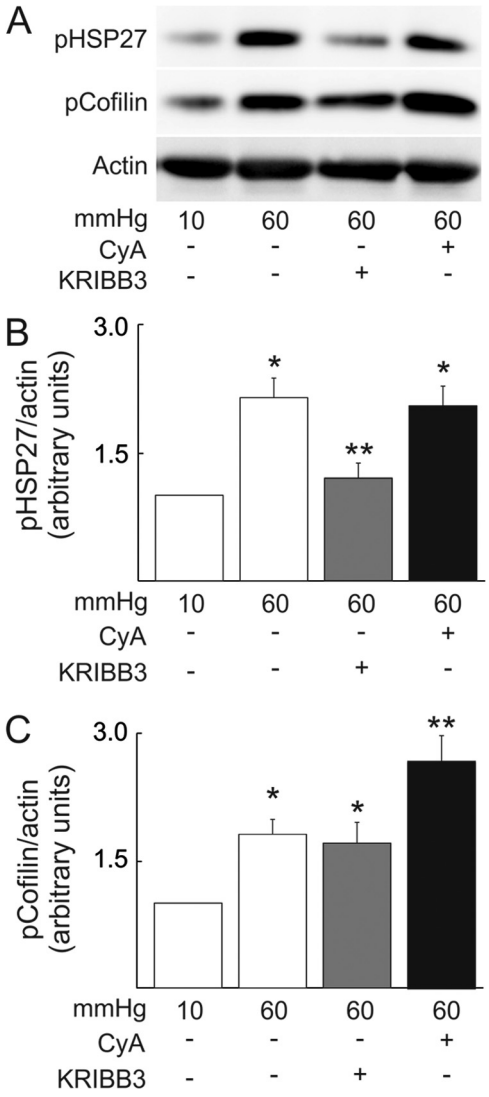

FIGURE 11. **KRIBB3 and cyclosporin A modulate HSP27-S82 and cofilin-S3 phosphorylation, respectively, in pressurized RMCAs.** *A*, representative Western blots of phospho-HSP27 and phospho-cofilin and corresponding levels of actin in each lane. *B* and *C*, mean levels ± S.E. of normalized (to actin) phosphoprotein content of RMCAs at 60 mm Hg ± KRIBB3 (10 μM) or CyA (10 μM), respectively, expressed as a fraction of the value at 10 mm Hg (*B* and *C*) (n = 5 blots with three arterial segments/sample). *, significantly different ($p < 0.05$) from value at 10 mm Hg. **, significantly different ($p < 0.05$) from value at 60 mm Hg.

the pressure-dependent increase in cofilin-S3 but had no effect on HSP27-S82 phosphorylation at this pressure. These modulators induced opposite effects on the myogenic response of RMCAs: addition of KRIBB3 (10 μM) elicited a vasodilation of ~35 μm (Fig. 12*A*), whereas CyA treatment (10 μM) was associated with a reduction in diameter of ~50 μm (Fig. 12*B*).

Finally, we assessed the direct contribution of cofilin and HSP27 to the cytoskeletal reorganization of RMCAs during the myogenic response by analyzing the effect of these phosphorylation modulators on the G-actin content at 60 mm Hg (Fig. 13). G-actin content in the presence of KRIBB3 was significantly elevated compared with that of untreated RMCAs at 60 mm Hg, but not different from that at 10 mm Hg, whereas treatment with CyA induced a significant decrease in G-actin content compared with both controls at 10 or 60 mm Hg ($p < 0.05$; n = 5 per group).

DISCUSSION

This study examined the role of thin filament regulatory proteins, calponin and caldesmon, and dynamic reorganization of the actin cytoskeleton in the myogenic response and agonist-evoked constriction of pressurized rat cerebral arteries. No change in thin filament protein phosphorylation was apparent, but a decline in G-actin content was observed in three situations of steady-state vasoconstriction not associated with a detectable augmentation of LC_{20} phosphorylation. A concomitant increase in the levels of cofilin-S3 and HSP27-S82 phosphorylation and a reduction in G-actin content were detected following pressure elevation, and these changes were blocked by inhibitors of ROK and PKC signaling. Blockade of HSP27 phosphorylation reversed the myogenic response and actin polymerization, whereas enhancement of cofilin phosphorylation induced further vasoconstriction and actin polymerization. Based on calculated levels of circumferential wall stress, we conclude that the fractional contribution of cytoskeletal reorganization to myogenic force development may be substantial, accounting for ~30% of maximal force generated at 120 mm Hg that is capable of effectively opposing the dilating influence of intravascular pressure to permit myogenic control of arterial diameter.

It is well accepted that LC_{20} phosphorylation is required for the activation of actomyosin MgATPase and cross-bridge cycling and that the level of phosphorylated LC_{20} determined by the relative activities of MLCK and MLCP is the principal determinant of force generation in smooth muscle (6, 57, 58). However, it is also apparent that the relationship between LC_{20} phosphorylation and force production is variable. MLCK activation, LC_{20} phosphorylation, and force are tightly coupled to the elevation in $[Ca^{2+}]_i$ during the initiation of contraction (59, 60), when changes in shortening velocity and force are proportional to the rise in phospho-LC_{20} content (57, 58, 61). How-

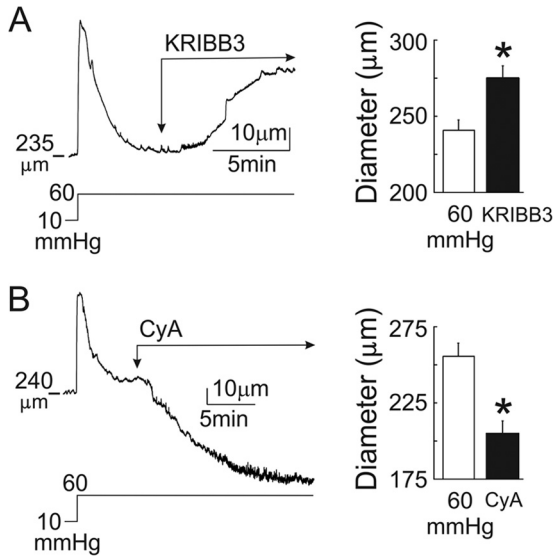

FIGURE 12. **Modulators of HSP27-S82 and cofilin-S3 phosphorylation alter RMCA myogenic response.** *A*, representative recording of RMCA diameter (*left panel*) and mean diameter (± S.E.; $n = 20$; *right panel*) during a step increase in pressure from 10 to 60 mm Hg followed by treatment with KRIBB3 (10 μM). *B*, representative recording of RMCA diameter (*left panel*) and mean diameter (± S.E.; $n = 20$; *right panel*) during a step increase in pressure from 10 to 60 mm Hg followed by treatment with CyA (10 μM). *, significantly different ($p < 0.05$) from value at 60 mm Hg.

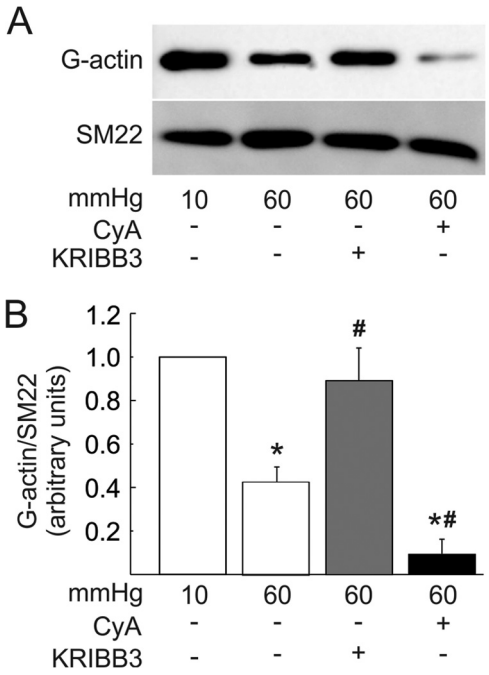

FIGURE 13. **Modulators of HSP27-S82 and cofilin-S3 phosphorylation induce changes in the G-actin content of pressurized RMCAs.** *A*, representative Western blot of G-actin and corresponding SM22 content in each lane. *B*, mean levels ± S.E. of G-actin normalized to SM22 of RMCAs at 60 mm Hg ± KRIBB3 (10 μM) or CyA I10 μM) expressed as a fraction of the value at 10 mm Hg ($n = 5$ blots with one arterial segment per sample). *, significantly different ($p < 0.05$) from value at 10 mm Hg. #, significantly different ($p < 0.05$) from value at 60 mm Hg.

ever, the level of LC_{20} phosphorylation declines markedly during sustained contraction, but force production is maintained (57, 58, 61, 62). Several mechanisms have been postulated to account for the lack of correlation between phospho-LC_{20} content and force in maintained contraction, including: (i) dephosphorylated "latch bridges" that cycle slowly or not at all (61); (ii) regulation of cross-bridge cycling by thin filament-associated proteins (23); (iii) a slow ADP off rate that is enhanced by the high force-induced strain on smooth muscle cross-bridges (63); and more recently, iv) dynamic reorganization of the actin cytoskeleton to enhance the efficiency of force transmission from the contractile apparatus to the cell membrane and extracellular matrix (24, 25, 56, 62, 64). Our findings support the view that intravascular pressure modulates the dynamics of actin polymerization via cellular signaling through ROK and PKC.

We failed to obtain evidence supporting a role for thin filament regulation in myogenic or 5-HT-evoked constriction. Calponin-mediated inhibition of actomyosin MgATPase and subsequent reduction in shortening velocity and force generation were previously shown to be prevented by phosphorylation of serine 175 by PKC or CaM kinase II (28, 51, 65, 66). Similarly, suppression of actomyosin MgATPase activity by caldesmon was blocked by phosphorylation of serine 789 by ERK1 in response to PKC activation (23, 67). Here, we failed to detect any change in calponin Ser-175 or caldesmon Ser-789 phosphorylation following pressurization (80–120 mm Hg) or in the presence of 5-HT and myogenic tone at 80 mm Hg.

There is substantial evidence to support the view that smooth muscle contraction and relaxation involve actin polymerization and depolymerization, respectively. For example, decreased G-actin content or a rise in F- to G-actin ratio, consistent with the utilization of G-actin and increased polymerization, was detected in tissues exposed to contractile agonists, elevated extracellular K^+ concentration, tissue stretch, osmotic volume change, or intravascular pressure (34–37, 56, 62, 64, 68–71). Force generation in these conditions was also shown to be affected by compounds that modify actin polymerization, such as cytochalasin D, jasplakinolide, and latrunculin B (19, 34–37, 68, 71–74). Here, we show that G-actin content was reduced by ~87% in a pressure-dependent manner between 10 and 120 mm Hg; no change was detected at 40 mm Hg, but significantly lower levels of G-actin were detected at 60, 80, and 120 mm Hg. Reduced G-actin content was also detected in the presence of 5-HT at 80 mm Hg (regardless of sequence), or during the initial development of myogenic tone at 60 mm Hg during equilibration. These data are consistent with previous reports, but by exploiting experimental conditions of vasoconstriction not accompanied by a detectable increase in LC_{20} phosphorylation, it was also possible to assess the relative importance of cytoskeletal reorganization to myogenic force generation.

Our approach, as illustrated in Fig. 14, was to determine the level of circumferential wall stress (force per unit area at midwall) at 10, 80, and 120 mm Hg based on our measurements of inner and outer diameter and Equation 1 (see "Experimental Procedures") from Coulson *et al.* (48) that considers RMCAs to be thick-walled, cylindrical tubes (*i.e.* ratio of radius to wall thickness is > 0.1). The respective levels of circumferential wall stress at 10 and 120 mm Hg approximate the minimum stress in the relaxed state and the maximal level of circumferential stress that can be opposed by myogenic constriction; *i.e.* force development above ~120 mm Hg is insufficient to offset pressure and forced dilation is observed (21). Given the observed lack of

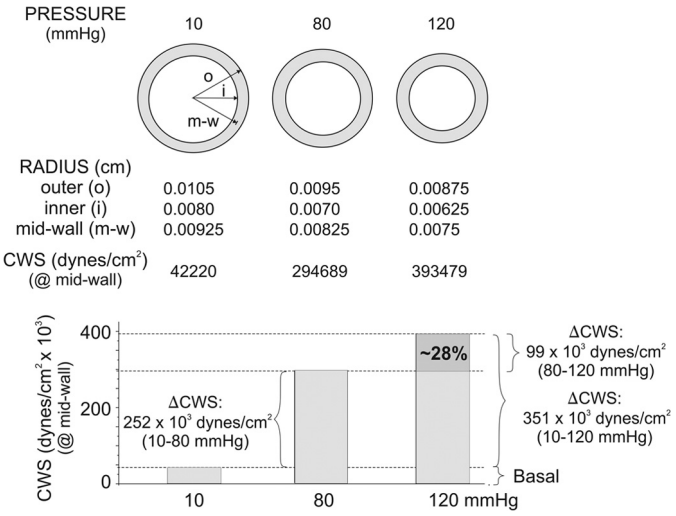

FIGURE 14. **Estimation of fractional contribution of cytoskeletal reorganization to force generation in the myogenic response based on levels of circumferential wall stress at 10, 80, and 120 mm Hg.** Diagrammatic representation and measured wall dimensions of RMCAs were employed to calculate circumferential wall stress (*CWS*) at 10, 80, and 120 mm Hg and determination of fractional change in circumferential wall stress between 80 and 120 mm Hg after subtraction of basal CWS at 10 mm Hg.

a detectable change in LC_{20} phosphorylation between 80 and 120 mm Hg, the difference in circumferential wall stress at these two pressures is indicative of the fractional increase in force that must be developed independent of an increase in LC_{20} phosphorylation and cross-bridge cycling to permit myogenic control of diameter. Based on this reasoning, ~30% of the total force generated to oppose intravascular pressure at 120 mm Hg may be dependent on cytoskeletal reorganization involving augmented actin polymerization (Fig. 14). The actual contribution to force generation likely exceeds 30% because (i) reorganization is not limited to the range of 80–120 mm Hg in RMCAs but also occurs between 40 and 80 mm Hg; however, over this lower pressure range, the fractional increase in force caused by reorganization cannot be distinguished from that caused by increased LC_{20} phosphorylation and cross-bridge cycling; (ii) force generation may also continue to increase with pressurization beyond 120 mm Hg, but any change in VSM tone is overwhelmed by intraluminal pressure and thus masked by forced dilatation; and (iii) the contribution of cytoskeletal reorganization is only considered at ≤5 min following pressurization. The cytoskeletal remodeling process associated with prolonged agonist-induced vasoconstriction was previously shown to be maintained, leading to a gradual increase in actin polymerization with time and, presumably, a greater fractional contribution to force generation (62, 75).

The cellular processes that orchestrate cytoskeletal remodeling in the myogenic response remain to be defined. Here, we show that the decline in G-actin and myogenic constriction at 120 mm Hg are accompanied by an increase in cofilin and HSP27 phosphorylation and that these changes are suppressed following inhibition of ROK or PKC. Specifically, H1152 and GF109203X reduced the decline in G-actin associated with pressurization, but H1152 blocked cofilin phosphorylation without affecting phospho-HSP27 content and GF109203X suppressed HSP27 phosphorylation but did not alter the level of phospho-cofilin. Cofilin contributes to actin dynamics by binding to and severing actin filaments, which favors depolymerization. This activity also provides soluble G-actin monomers and short, capped actin filaments with barbed ends that are free to act as nucleation sites for new filament growth (76–78). Cofilin activity is suppressed following phosphorylation of Ser-3 by LIM kinase (79), and LIM kinase activity is in turn dependent on phosphorylation by ROK or p21-activated kinases (PAK1 and 4) downstream of RhoA and Cdc42, respectively (79). In contrast, HSP27 may suppress actin polymerization by directly binding to G-actin (80, 81) or by capping the barbed ends of F-actin which prevents filament elongation (82), but the mechanism is controversial (83). Phosphorylation of HSP27 blocks its G-actin binding and capping activity, but phospho-HSP27 may also bind to and stabilize F-actin filaments (84). HSP27 phosphorylation by MAP kinase-activated protein kinase 2 or 3 in response to upstream regulation by p38 MAP kinase is the most widely identified regulatory pathway (85, 86), but PKC has also been demonstrated to phosphorylate HSP27 (87, 88). Actin dynamics in the myogenic response may therefore require parallel activation of (i) RhoA-ROK to promote actin polymerization by stimulating LIM kinase and subsequent suppression of cofilin-mediated actin severing and depolymerization and (ii) PKC-mediated activation by diacylglycerol generated through pressure-evoked phospholipase C activity (89) and subsequent phosphorylation of HSP27 to promote polymerization. The involvement of ROK in the regulation of cofilin activity represents the second potential role for this kinase in the myogenic response, the first being the phosphorylation of MYPT1 and suppression of MLCP activity leading to Ca^{2+} sensitization (18, 52). That PKC contributes to the regulation of force in the myogenic response is well recognized (20, 21, 90–93), but the mechanism(s) involved has not been established with certainty. Previous studies postulated that PKC might phosphorylate CPI-17 and/or MYPT1, leading to an inhibition of MLCP activity, Ca^{2+} sensitization of the contractile filaments, increased LC_{20} phosphorylation, and greater force at constant $[Ca^{2+}]_i$ (6, 8, 94). However, this is unlikely because no evidence of a pressure-dependent increase in the level of phospho-CPI-17 or PKC-dependent MYPT1 phosphorylation was detected in the myogenic response of rat cerebral or gracilis arteries (18, 19, 52). That the pressure-dependent increase in HSP27 phosphorylation and decline in G-actin content were blocked by GF109203X treatment in this study indicates that PKC inhibitors may suppress myogenic constriction through inhibition of PKC-mediated HSP27 phosphorylation and actin polymerization.

KRIBB3 and CyA effects on HSP27 and cofilin phosphorylation levels, myogenic constriction, and G-actin content levels of RMCAs serve as additional evidence that these proteins play direct roles in the actin reorganization process in the myogenic response. KRIBB3 inhibits PKC-dependent HSP27 phosphorylation and migration in adenocarcinoma cell lines (95, 96). CyA is a phosphatase 2B inhibitor that prevents cofilin dephosphorylation (44, 97). Here, KRIBB3 and CyA treatments were used at 60 mm Hg to provide a wider range for potential changes of arterial diameter, G-actin content, and HSP27 and cofilin phosphorylation levels. KRIBB3, by preventing HSP27 phosphorylation and its uncapping from the actin filament, induced a loss

of myogenic tone and blocked the pressure-induced reduction in G-actin content. CyA, on the other hand, prevented phosphatase 2B-mediated cofilin dephosphorylation and its actin severing function, thus inducing contraction of the artery, as reported for other vascular beds (98). It also evoked a greater decrease in G-actin content and an increase in cofilin-S3, but not HSP27-S82 phosphorylation. The lack of effect on phospho-HSP27-S82 is consistent with previous findings that HSP27 is dephosphorylated by PP2A, but not PP2B (99).

Our findings indicate that the regulation of cytoskeletal reorganization in the myogenic response may differ from that in stretch-, agonist-, and KCl-evoked contraction. For example, contraction of portal vein smooth muscle in response to stretch was accompanied by a ROK-mediated increase in cofilin phosphorylation and F:G-actin ratio (100). However, the time required for these changes (>1 h) was considerably longer than observed here for myogenic constriction (3–5 min). Also, a reduced level of phospho-cofilin, rather than an increase, was found to accompany the rise in F:G-actin ratio in airway and carotid arterial smooth muscle tissues contracted by acetylcholine or elevated external K^+ concentration (44, 56). We assessed this possibility by treating RMCAs with 5-HT at 10 mm Hg, but an increase, not a decrease, in cofilin phosphorylation was detected. The mechanism of HSP27 inhibition in the myogenic response may also differ; specifically, HSP27 phosphorylation in agonist- and/or stretch-evoked contraction of airway smooth muscle, mesenteric arteries, and rabbit facial vein tissues was shown to be sensitive to inhibition of p38 MAP kinase and/or ROK inhibition rather than PKC (46, 101, 102). The reason(s) for these varied findings is not known, but an intriguing possibility is that cytoskeletal reorganization in the myogenic response is mediated by a different complement of signaling pathway(s) and membrane adhesion proteins compared with those involved in stretch-, agonist-, or KCl-evoked isometric contraction of VSMCs. A better understanding of processes contributing to actin dynamics in the myogenic response is required to permit definitive conclusions regarding the reason(s) for stimulus-dependent differences in the mechanism of cytoskeletal reorganization.

REFERENCES

1. Faraci, F. M., and Heistad, D. D. (1990) Regulation of large cerebral arteries and cerebral microvascular pressure. *Circ. Res.* **66,** 8–17
2. Davis, M. J., and Hill, M. A. (1999) Signaling mechanisms underlying the vascular myogenic response. *Physiol. Rev.* **79,** 387–423
3. Hamel, E. (2006) Perivascular nerves and the regulation of cerebrovascular tone. *J. Appl. Physiol.* **100,** 1059–1064
4. Straub, S. V., and Nelson, M. T. (2007) Astrocytic calcium signaling: the information currency coupling neuronal activity to the cerebral microcirculation. *Trends Cardiovasc. Med.* **17,** 183–190
5. Somlyo, A. P., and Somlyo, A. V. (1994) Signal transduction and regulation in smooth muscle. *Nature* **372,** 231–236
6. Somlyo, A. P., and Somlyo, A. V. (2003) Ca^{2+} sensitivity of smooth muscle and nonmuscle myosin II: modulated by G proteins, kinases, and myosin phosphatase. *Physiol. Rev.* **83,** 1325–1358
7. Somlyo, A. P., and Somlyo, A. V. (2004) Signal transduction through the RhoA/Rho-kinase pathway in smooth muscle. *J. Muscle Res. Cell Motil.* **25,** 613–615
8. Hirano, K. (2007) Current topics in the regulatory mechanism underlying the Ca^{2+} sensitization of the contractile apparatus in vascular smooth muscle. *J. Pharmacol. Sci.* **104,** 109–115
9. Cole, W. C., and Welsh, D. G. (2011) Role of myosin light chain kinase and myosin light chain phosphatase in the resistance arterial myogenic response to intravascular pressure. *Arch. Biochem. Biophys.* **510,** 160–173
10. Feng, J., Ito, M., Ichikawa, K., Isaka, N., Nishikawa, M., Hartshorne, D. J., and Nakano, T. (1999) Inhibitory phosphorylation site for Rho-associated kinase on smooth muscle myosin phosphatase. *J. Biol. Chem.* **274,** 37385–37390
11. Velasco, G., Armstrong, C., Morrice, N., Frame, S., and Cohen, P. (2002) Phosphorylation of the regulatory subunit of smooth muscle protein phosphatase 1M at Thr850 induces its dissociation from myosin. *FEBS Lett.* **527,** 101–104
12. Murányi, A., Derkach, D., Erdodi, F., Kiss, A., Ito, M., and Hartshorne, D. J. (2005) Phosphorylation of Thr695 and Thr850 on the myosin phosphatase target subunit: inhibitory effects and occurrence in A7r5 cells. *FEBS Lett.* **579,** 6611–6615
13. Eto, M. (2009) Regulation of cellular protein phosphatase-1 (PP1) by phosphorylation of the CPI-17 family, C-kinase-activated PP1 inhibitors. *J. Biol. Chem.* **284,** 35273–35277
14. Knot, H. J., and Nelson, M. T. (1998) Regulation of arterial diameter and wall $[Ca^{2+}]$ in cerebral arteries of rat by membrane potential and intravascular pressure. *J. Physiol.* **508,** 199–209
15. Mufti, R. E., Brett, S. E., Tran, C. H., Abd El-Rahman, R., Anfinogenova, Y., El-Yazbi, A., Cole, W. C., Jones, P. P., Chen, S. R., and Welsh, D. G. (2010) Intravascular pressure augments cerebral arterial constriction by inducing voltage-insensitive Ca^{2+} waves. *J. Physiol.* **588,** 3983–4005
16. Jaggar, J. H. (2001) Intravascular pressure regulates local and global Ca^{2+} signaling in cerebral artery smooth muscle cells. *Am. J. Physiol. Cell Physiol.* **281,** C439–C448
17. Zou, H., Ratz, P. H., and Hill, M. A. (1995) Role of myosin phosphorylation and $[Ca^{2+}]_i$ in myogenic reactivity and arteriolar tone. *Am. J. Physiol.* **269,** H1590–H1596
18. Johnson, R. P., El-Yazbi, A. F., Takeya, K., Walsh, E. J., Walsh, M. P., and Cole, W. C. (2009) Ca^{2+} sensitization via phosphorylation of myosin phosphatase targeting subunit at threonine-855 by Rho kinase contributes to the arterial myogenic response. *J. Physiol.* **587,** 2537–2553
19. Moreno-Domínguez, A., Colinas, O., El-Yazbi, A., Walsh, E. J., Hill, M. A., Walsh, M. P., and Cole, W. C. (2013) Ca^{2+} sensitization due to myosin light chain phosphatase inhibition and cytoskeletal reorganization in the myogenic response of skeletal muscle resistance arteries. *J. Physiol.* **591,** 1235–1250
20. Hill, M. A., Falcone, J. C., and Meininger, G. A. (1990) Evidence for protein kinase C involvement in arteriolar myogenic reactivity. *Am. J. Physiol.* **259,** H1586–H1594
21. Osol, G., Laher, I., and Cipolla, M. (1991) Protein kinase C modulates basal myogenic tone in resistance arteries from the cerebral circulation. *Circ. Res.* **68,** 359–367
22. Walsh, M. P., and Cole, W. C. (2013) The role of actin filament dynamics in the myogenic response of cerebral resistance arteries. *J. Cereb. Blood Flow Metab.* **33,** 1–12
23. Morgan, K. G., and Gangopadhyay, S. S. (2001) Invited review: cross-bridge regulation by thin filament-associated proteins. *J. Appl. Physiol.* **91,** 953–962
24. Gerthoffer, W. T. (2005) Actin cytoskeletal dynamics in smooth muscle contraction. *Can. J. Physiol. Pharmacol.* **83,** 851–856
25. Gunst, S. J., and Zhang, W. (2008) Actin cytoskeletal dynamics in smooth muscle: a new paradigm for the regulation of smooth muscle contraction. *Am. J. Physiol. Cell Physiol.* **295,** C576–C587
26. Jin, J. P., Walsh, M. P., Sutherland, C., and Chen, W. (2000) A role for serine-175 in modulating the molecular conformation of calponin. *Biochem. J.* **350,** 579–588
27. Kaneko, T., Amano, M., Maeda, A., Goto, H., Takahashi, K., Ito, M., and Kaibuchi, K. (2000) Identification of calponin as a novel substrate of Rho-kinase. *Biochem. Biophys. Res. Commun.* **273,** 110–116
28. Walsh, M. P., Horowitz, A., Clément-Chomienne, O., Andrea, J. E., Allen, B. G., and Morgan, K. G. (1996) Protein kinase C mediation of Ca^{2+}-independent contractions of vascular smooth muscle. *Biochem. Cell Biol.* **74,** 485–502
29. Horowitz, A., Clément-Chomienne, O., Walsh, M. P., Tao, T., Katsuyama, H., and Morgan, K. G. (1996) Effects of calponin on force generation

by single smooth muscle cells. *Am. J. Physiol.* **270,** H1858–H1863
30. Malmqvist, U., Trybus, K. M., Yagi, S., Carmichael, J., and Fay, F. S. (1997) Slow cycling of unphosphorylated myosin is inhibited by calponin, thus keeping smooth muscle relaxed. *Proc. Natl. Acad. Sci. U.S.A.* **94,** 7655–7660
31. Dessy, C., Kim, I., Sougnez, C. L., Laporte, R., and Morgan, K. G. (1998) A role for MAP kinase in differentiated smooth muscle contraction evoked by α-adrenoceptor stimulation. *Am. J. Physiol.* **275,** C1081–C1086
32. Xiao, D., Pearce, W. J., Longo, L. D., and Zhang, L. (2004) ERK-mediated uterine artery contraction: role of thick and thin filament regulatory pathways. *Am. J. Physiol. Heart Circ Physiol.* **286,** H1615–H1622
33. Yamin, R., and Morgan, K. G. (2012) Deciphering actin cytoskeletal function in the contractile vascular smooth muscle cell. *J. Physiol.* **590,** 4145–4154
34. Cipolla, M. J., and Osol, G. (1998) Vascular smooth muscle actin cytoskeleton in cerebral artery forced dilatation. *Stroke* **29,** 1223–1228
35. Cipolla, M. J., Gokina, N. I., and Osol, G. (2002) Pressure-induced actin polymerization in vascular smooth muscle as a mechanism underlying myogenic behavior. *FASEB J.* **16,** 72–76
36. Gokina, N. I., and Osol, G. (2002) Actin cytoskeletal modulation of pressure-induced depolarization and Ca^{2+} influx in cerebral arteries. *Am. J. Physiol. Heart Circ Physiol.* **282,** H1410–H1420
37. Flavahan, N. A., Bailey, S. R., Flavahan, W. A., Mitra, S., and Flavahan, S. (2005) Imaging remodeling of the actin cytoskeleton in vascular smooth muscle cells after mechanosensitive arteriolar constriction. *Am. J. Physiol. Heart Circ Physiol.* **288,** H660–H669
38. Osol, G., Brekke, J. F., McElroy-Yaggy, K., and Gokina, N. I. (2002) Myogenic tone, reactivity, and forced dilatation: a three-phase model of *in vitro* arterial myogenic behavior. *Am. J. Physiol. Heart Circ Physiol.* **283,** H2260–H2267
39. Gerthoffer, W. T., and Gunst, S. J. (2001) Invited review: focal adhesion and small heat shock proteins in the regulation of actin remodeling and contractility in smooth muscle. *J. Appl. Physiol.* **91,** 963–972
40. Kim, H. R., Gallant, C., Leavis, P. C., Gunst, S. J., and Morgan, K. G. (2008) Cytoskeletal remodeling in differentiated vascular smooth muscle is actin isoform dependent and stimulus dependent. *Am. J. Physiol. Cell Physiol.* **295,** C768–C778
41. Gallant, C., Appel, S., Graceffa, P., Leavis, P., Lin, J. J., Gunning, P. W., Schevzov, G., Chaponnier, C., DeGnore, J., Lehman, W., and Morgan, K. G. (2011) Tropomyosin variants describe distinct functional subcellular domains in differentiated vascular smooth muscle cells. *Am. J. Physiol. Cell Physiol.* **300,** C1356–C1365
42. Pavalko, F. M., Adam, L. P., Wu, M. F., Walker, T. L., and Gunst, S. J. (1995) Phosphorylation of dense-plaque proteins talin and paxillin during tracheal smooth muscle contraction. *Am. J. Physiol.* **268,** C563–C571
43. Zhang, W., Wu, Y., Du, L., Tang, D. D., and Gunst, S. J. (2005) Activation of the Arp2/3 complex by N-WASp is required for actin polymerization and contraction in smooth muscle. *Am. J. Physiol. Cell Physiol.* **288,** C1145–C1160
44. Zhao, R., Du, L., Huang, Y., Wu, Y., and Gunst, S. J. (2008) Actin depolymerization factor/cofilin activation regulates actin polymerization and tension development in canine tracheal smooth muscle. *J. Biol. Chem.* **283,** 36522–36531
45. Komalavilas, P., Penn, R. B., Flynn, C. R., Thresher, J., Lopes, L. B., Furnish, E. J., Guo, M., Pallero, M. A., Murphy-Ullrich, J. E., and Brophy, C. M. (2008) The small heat shock-related protein, HSP20, is a cAMP-dependent protein kinase substrate that is involved in airway smooth muscle relaxation. *Am. J. Physiol. Lung Cell Mol Physiol.* **294,** L69–L78
46. Srinivasan, R., Forman, S., Quinlan, R. A., Ohanian, J., and Ohanian, V. (2008) Regulation of contractility by Hsp27 and Hic-5 in rat mesenteric small arteries. *Am. J. Physiol. Heart Circ Physiol.* **294,** H961–H969
47. Kim, H. R., Graceffa, P., Ferron, F., Gallant, C., Boczkowska, M., Dominguez, R., Morgan, K. G. (2010) Actin polymerization in differentiated vascular smooth muscle cells requires vasodilator-stimulated phosphoprotein. *Am. J. Physiol. Cell Physiol.* **298,** C559–C571
48. Coulson, R. J., Chesler, N. C., Vitullo, L., and Cipolla, M. J. (2002) Effects of ischemia and myogenic activity on active and passive mechanical properties of rat cerebral arteries. *Am. J. Physiol. Heart Circ Physiol.* **283,** H2268–H2275
49. Takeya, K., Loutzenhiser, K., Shiraishi, M., Loutzenhiser, R., and Walsh, M. P. (2008) A highly sensitive technique to measure myosin regulatory light chain phosphorylation: the first quantification in renal arterioles. *Am. J. Physiol. Renal Physiol.* **294,** F1487–F1492
50. Walsh, M. P., Thornbury, K., Cole, W. C., Sergeant, G., Hollywood, M., and McHale, N. (2011) Rho-associated kinase plays a role in rabbit urethral smooth muscle contraction, but not via enhanced myosin light chain phosphorylation. *Am. J. Physiol. Renal Physiol.* **300,** F73–F85
51. Winder, S. J., and Walsh, M. P. (1990) Smooth muscle calponin. Inhibition of actomyosin MgATPase and regulation by phosphorylation. *J. Biol. Chem.* **265,** 10148–10155
52. El-Yazbi, A. F., Johnson, R. P., Walsh, E. J., Takeya, K., Walsh, M. P., and Cole, W. C. (2010) Pressure-dependent contribution of Rho kinase-mediated calcium sensitization in serotonin-evoked vasoconstriction of rat cerebral arteries. *J. Physiol.* **588,** 1747–1762
53. Chen, X., Pavlish, K., and Benoit, J. N. (2008) Myosin phosphorylation triggers actin polymerization in vascular smooth muscle. *Am. J. Physiol. Heart Circ Physiol.* **295,** H2172–H2177
54. Eddinger, T. J., Meer, D. P., Miner, A. S., Meehl, J., Rovner, A. S., and Ratz, P. H. (2007) Potent inhibition of arterial smooth muscle tonic contractions by the selective myosin II inhibitor, blebbistatin. *J. Pharmacol. Exp. Ther.* **320,** 865–870
55. Bitar, K. N. (2002) HSP27 phosphorylation and interaction with actin-myosin in smooth muscle contraction. *Am. J. Physiol. Gastrointest. Liver Physiol.* **282,** G894–G903
56. Tejani, A. D., Walsh, M. P., and Rembold, C. M. (2011) Tissue length modulates "stimulated actin polymerization," force augmentation, and the rate of swine carotid arterial contraction. *Am. J. Physiol. Cell Physiol.* **301,** C1470–C1478
57. Kamm, K. E., and Stull, J. T. (1985) The function of myosin and myosin light chain kinase phosphorylation in smooth muscle. *Annu. Rev. Pharmacol. Toxicol.* **25,** 593–620
58. Ratz, P. H., Hai, C. M., and Murphy, R. A. (1989) Dependence of stress on cross-bridge phosphorylation in vascular smooth muscle. *Am. J. Physiol.* **256,** C96–C100
59. Wier, W. G., Rizzo, M. A., Raina, H., and Zacharia, J. (2008) A technique for simultaneous measurement of Ca^{2+}, FRET fluorescence and force in intact mouse small arteries. *J. Physiol.* **586,** 2437–2443
60. Ding, H. L., Ryder, J. W., Stull, J. T., and Kamm, K. E. (2009) Signaling processes for initiating smooth muscle contraction upon neural stimulation. *J. Biol. Chem.* **284,** 15541–15548
61. Murphy, R. A., and Rembold, C. M. (2005) The latch-bridge hypothesis of smooth muscle contraction. *Can. J. Physiol. Pharmacol.* **83,** 857–864
62. Rembold, C. M., Tejani, A. D., Ripley, M. L., and Han, S. (2007) Paxillin phosphorylation, actin polymerization, noise temperature, and the sustained phase of swine carotid artery contraction. *Am. J. Physiol. Cell Physiol.* **293,** C993–C1002
63. Khromov, A. S., Webb, M. R., Ferenczi, M. A., Trentham, D. R., Somlyo, A. P., and Somlyo, A. V. (2004) Myosin regulatory light chain phosphorylation and strain modulate adenosine diphosphate release from smooth muscle myosin. *Biophys. J.* **86,** 2318–2328
64. Tejani, A. D., and Rembold, C. M. (2010) Force augmentation and stimulated actin polymerization in swine carotid artery. *Am. J. Physiol. Cell Physiol.* **298,** C182–C190
65. Jaworowski, A., Anderson, K. I., Arner, A., Engström, M., Gimona, M., Strasser, P., and Small, J. V. (1995) Calponin reduces shortening velocity in skinned taenia coli smooth muscle fibres. *FEBS Lett.* **365,** 167–171
66. Pohl, J., Winder, S. J., Allen, B. G., Walsh, M. P., Sellers, J. R., and Gerthoffer, W. T. (1997) Phosphorylation of calponin in airway smooth muscle. *Am. J. Physiol.* **272,** L115–L123
67. Marston, S. B., and Redwood, C. S. (1992) Inhibition of actin-tropomyosin activation of myosin MgATPase activity by the smooth muscle regulatory protein caldesmon. *J. Biol. Chem.* **267,** 16796–16800
68. Shaw, L., Ahmed, S., Austin, C., and Taggart, M. J. (2003) Inhibitors of actin filament polymerisation attenuate force but not global intracellular calcium in isolated pressurised resistance arteries. *J. Vasc. Res.* **40,** 1–10
69. Kim, Y. S., Immink, R. V., Stok, W. J., Karemaker, J. M., Secher, N. H., and

van Lieshout, J. J. (2008) Dynamic cerebral autoregulatory capacity is affected early in Type 2 diabetes. *Clin. Sci.* (*Lond.*) **115,** 255–262
70. Koltsova, S. V., Gusakova, S. V., Anfinogenova, Y. J., Baskakov, M. B., and Orlov, S. N. (2008) Vascular smooth muscle contraction evoked by cell volume modulation: role of the cytoskeleton network. *Cell Physiol. Biochem.* **21,** 29–36
71. Ohanian, V., Gatfield, K., and Ohanian, J. (2005) Role of the actin cytoskeleton in G-protein-coupled receptor activation of PYK2 and paxillin in vascular smooth muscle. *Hypertension* **46,** 93–99
72. Saito, S. Y., Hori, M., Ozaki, H., and Karaki, H. (1996) Cytochalasin D inhibits smooth muscle contraction by directly inhibiting contractile apparatus. *J. Smooth Muscle Res.* **32,** 51–60
73. Dowell, M. L., Lakser, O. J., Gerthoffer, W. T., Fredberg, J. J., Stelmack, G. L., Halayko, A. J., Solway, J., and Mitchell, R. W. (2005) Latrunculin B increases force fluctuation-induced relengthening of ACh-contracted, isotonically shortened canine tracheal smooth muscle. *J. Appl. Physiol.* **98,** 489–497
74. McVicker, C. G., Leung, S. Y., Kanabar, V., Moir, L. M., Mahn, K., Chung, K. F., and Hirst, S. J. (2007) Repeated allergen inhalation induces cytoskeletal remodeling in smooth muscle from rat bronchioles. *Am. J. Respir. Cell Mol. Biol.* **36,** 721–727
75. Staiculescu, M. C., Galiñanes, E. L., Zhao, G., Ulloa, U., Jin, M., Beig, M. I., Meininger, G. A., and Martinez-Lemus, L. A. (2013) Prolonged vasoconstriction of resistance arteries involves vascular smooth muscle actin polymerization leading to inward remodelling. *Cardiovasc. Res.* **98,** 428–436
76. Carlier, M. F., Laurent, V., Santolini, J., Melki, R., Didry, D., Xia, G. X., Hong, Y., Chua, N. H., and Pantaloni, D. (1997) Actin depolymerizing factor (ADF/cofilin) enhances the rate of filament turnover: implication in actin-based motility. *J. Cell Biol.* **136,** 1307–1322
77. Bamburg, J. R. (1999) Proteins of the ADF/cofilin family: essential regulators of actin dynamics. *Annu. Rev. Cell Dev. Biol.* **15,** 185–230
78. Ichetovkin, I., Grant, W., and Condeelis, J. (2002) Cofilin produces newly polymerized actin filaments that are preferred for dendritic nucleation by the Arp2/3 complex. *Curr. Biol.* **12,** 79–84
79. Bernard, O. (2007) Lim kinases, regulators of actin dynamics. *Int. J. Biochem. Cell Biol.* **39,** 1071–1076
80. Wieske, M., Benndorf, R., Behlke, J., Dölling, R., Grelle, G., Bielka, H., and Lutsch, G. (2001) Defined sequence segments of the small heat shock proteins HSP25 and αB-crystallin inhibit actin polymerization. *Eur. J. Biochem.* **268,** 2083–2090
81. Wang, H., Robinson, R. C., and Burtnick, L. D. (2010) The structure of native G-actin. *Cytoskeleton* **67,** 456–465
82. Miron, T., Vancompernolle, K., Vandekerckhove, J., Wilchek, M., and Geiger, B. (1991) A 25-kD inhibitor of actin polymerization is a low molecular mass heat shock protein. *J. Cell Biol.* **114,** 255–261
83. Mymrikov, E. V., Seit-Nebi, A. S., and Gusev, N. B. (2011) Large potentials of small heat shock proteins. *Physiol. Rev.* **91,** 1123–1159
84. Mounier, N., and Arrigo, A. P. (2002) Actin cytoskeleton and small heat shock proteins: how do they interact? *Cell Stress Chaperones* **7,** 167–176
85. Stokoe, D., Engel, K., Campbell, D. G., Cohen, P., and Gaestel, M. (1992) Identification of MAPKAP kinase 2 as a major enzyme responsible for the phosphorylation of the small mammalian heat shock proteins. *FEBS Lett.* **313,** 307–313
86. McLaughlin, M. M., Kumar, S., McDonnell, P. C., Van Horn, S., Lee, J. C., Livi, G. P., and Young, P. R. (1996) Identification of mitogen-activated protein (MAP) kinase-activated protein kinase-3, a novel substrate of CSBP p38 MAP kinase. *J. Biol. Chem.* **271,** 8488–8492
87. Maizels, E. T., Peters, C. A., Kline, M., Cutler, R. E. Jr., Shanmugam, M., and Hunzicker-Dunn, M. (1998) Heat-shock protein-25/27 phosphorylation by the delta isoform of protein kinase C. *Biochem. J.* **332,** 703–712
88. Kato, K., Ito, H., Iwamoto, I., Lida, K., and Inaguma, Y. (2001) Protein kinase inhibitors can suppress stress-induced dissociation of Hsp27. *Cell Stress Chaperones* **6,** 16–20
89. Osol, G., Laher, I., and Kelley, M. (1993) Myogenic tone is coupled to phospholipase C and G protein activation in small cerebral arteries. *Am. J. Physiol.* **265,** H415–H420
90. Karibe, A., Watanabe, J., Horiguchi, S., Takeuchi, M., Suzuki, S., Funakoshi, M., Katoh, H., Keitoku, M., Satoh, S., and Shirato, K. (1997) Role of cytosolic Ca^{2+} and protein kinase C in developing myogenic contraction in isolated rat small arteries. *Am. J. Physiol.* **272,** H1165–H1172
91. Bakker, E. N., Kerkhof, C. J., and Sipkema, P. (1999) Signal transduction in spontaneous myogenic tone in isolated arterioles from rat skeletal muscle. *Cardiovasc. Res.* **41,** 229–236
92. Dessy, C., Matsuda, N., Hulvershorn, J., Sougnez, C. L., Sellke, F. W., and Morgan, K. G. (2000) Evidence for involvement of the PKC-α isoform in myogenic contractions of the coronary microcirculation. *Am. J. Physiol. Heart Circ Physiol.* **279,** H916–H923
93. Massett, M. P., Ungvari, Z., Csiszar, A., Kaley, G., and Koller, A. (2002) Different roles of PKC and MAP kinases in arteriolar constrictions to pressure and agonists. *Am. J. Physiol. Heart Circ Physiol.* **283,** H2282–H2287
94. Dimopoulos, G. J., Semba, S., Kitazawa, K., Eto, M., and Kitazawa, T. (2007) Ca^{2+}-dependent rapid Ca^{2+} sensitization of contraction in arterial smooth muscle. *Circ. Res.* **100,** 121–129
95. Shin, K. D., Lee, M. Y., Shin, D. S., Lee, S., Son, K. H., Koh, S., Paik, Y. K., Kwon, B. M., and Han, D. C. (2005) Blocking tumor cell migration and invasion with biphenyl isoxazole derivative KRIBB3, a synthetic molecule that inhibits Hsp27 phosphorylation. *J. Biol. Chem.* **280,** 41439–41448
96. Hsu, H. S., Lin, J. H., Huang, W. C., Hsu, T. W., Su, K., Chiou, S. H., Tsai, Y. T., and Hung, S. C. (2011) Chemoresistance of lung cancer stemlike cells depends on activation of Hsp27. *Cancer* **117,** 1516–1528
97. Meberg, P. J., Ono, S., Minamide, L. S., Takahashi, M., and Bamburg, J. R. (1998) Actin depolymerizing factor and cofilin phosphorylation dynamics: response to signals that regulate neurite extension. *Cell. Motil. Cytoskeleton* **39,** 172–190
98. Kaye, D., Thompson, J., Jennings, G., and Esler, M. (1993) Cyclosporine therapy after cardiac transplantation causes hypertension and renal vasoconstriction without sympathetic activation. *Circulation* **88,** 1101–1109
99. Cairns, J., Qin, S., Philp, R., Tan, Y. H., and Guy, G. R. (1994) Dephosphorylation of the small heat shock protein Hsp27 in vivo by protein phosphatase 2A. *J. Biol. Chem.* **269,** 9176–9183
100. Albinsson, S., Nordström, I., and Hellstrand, P. (2004) Stretch of the vascular wall induces smooth muscle differentiation by promoting actin polymerization. *J. Biol. Chem.* **279,** 34849–34855
101. Larsen, J. K., Yamboliev, I. A., Weber, L. A., and Gerthoffer, W. T. (1997) Phosphorylation of the 27-kDa heat shock protein via p38 MAP kinase and MAPKAP kinase in smooth muscle. *Am. J. Physiol.* **273,** L930–L940
102. Dubroca, C., You, D., Lévy, B. I., Loufrani, L., and Henrion, D. (2005) Involvement of RhoA/Rho kinase pathway in myogenic tone in the rabbit facial vein. *Hypertension* **45,** 974–979